A Modeling Study of the Cloud-Topped Marine Boundary Layer

Thomas A. Guinn

Colorado State University

DEPARTMENT OF ATMOSPHERIC SCIENCE

PAPER NO. 458

A MODELING STUDY OF THE CLOUD-TOPPED MARINE BOUNDARY LAYER

by

Thomas A. Guinn

Department of Atmospheric Science
Colorado State University
Fort Collins, CO 80523

This research was supported by the Marine Meteorology Program of the Office of Naval Research under contract N00014-87-K-0228

Atmospheric Science Paper No. 458

November 1989

Abstract

A coupled convective-radiative, boundary-layer model of marine stratocumulus clouds is presented. The model, which slightly generalizes Lilly's (1968) cloud-topped mixed-layer model, has as dependent variables the cloud-top height, the cloud-base height, mixed-layer equivalent potential temperature and total water mixing ratio, the turbulent fluxes of equivalent potential temperature, total water mixing ratio, and virtual potential temperature, the cloud-top jumps of equivalent potential temperature and total water mixing ratio, the cloud-top temperature, and the net radiative flux divergence at cloud top and in the mixed layer.

The model has been programmed for both the steady-state and time dependent cases using two different closure assumptions. Closure method one is a weighted average of Lilly's (1968) maximum and minimum entrainment assumptions. Closure method two assumes the ratio of the integral buoyant energy dissipation to the buoyant energy production to be constant. Experiments were performed to determine which closure method produced the best results, and to simulate the observed diurnal thinning of the marine stratocumulus clouds.

Results indicate that closure method two provides a more realistic representation of the observed marine boundary layer than does closure method one for both the steady-state case and the time dependent case. Results from the diurnal cycle simulations indicate that it is possible to simulate the observed thinning trend of the stratocumulus cloud layer although the magnitude of the thinning is less than observed. Results also indicate that thin clouds are more susceptible to thinning than are thick clouds.

Acknowledgements

I would like to extend my sincerest gratitude to Dr. Wayne Schubert for all of his guidance. His tremendous skill, insight, and patience as both an advisor and an instructor aided immeasurably in the completion of this report. I would also like to thank Dr. Stephen Cox and Dr. Robert Meroney for their generous evaluations and comments. I am grateful to Mr. Paul Ciesielski for all his help with my computing and programming. Thanks are also due to Ms. Jenny Martin for all of her assistance in the preparation of this manuscript.

I would also like to thank my wife Jolene for all the support and understanding she provided me during the many late nights and long hours that occurred while I worked on both my course studies and my research.

Lastly, I would like to thank the United States Air Force and the Air Force Institute of Technology (AFIT) program for providing me with this wonderful opportunity.

This report was supported by the Marine Meteorology Program of the Office of Naval Research under contract N00014-87-K-0228.

Table of Contents

List of Figures

List of Tables

Chapter 1

INTRODUCTION

In a field which gains the majority of its notoriety from the prediction of life threatening weather such as hurricanes, tornadoes, and lightning it seems odd that marine stratocumulus clouds would need to be studied. However, when one considers that the globally averaged stratiform cloud coverage is on the order of 12–15% (Randall, 1985a), their impact on the planetary albedo and therefore the global climate becomes of great importance. It has even been calculated that a 4% increase in the global coverage of the earth by stratocumulus type clouds could actually offset the the 2–3 K predicted rise in global temperature stemming from the carbon dioxide greenhouse effect (Randall *et al.*, 1984). The role of stratocumulus clouds in the climate of our planet does not end with radiative effects. Stratocumulus clouds also play a major role in the turbulent heat and moisture exchange between the boundary layer and the free atmosphere. Clearly, then, if the global climate is to be accurately simulated an understanding of marine stratiform clouds must be acquired.

Marine stratocumulus are typically found over the cool waters of the subtropic oceans where large scale sinking motion suppresses strong convection, near the eastern edges of the subtropical highs. The five principal areas where marine stratocumulus exist are coastal Oregon, California and Mexico, coastal Equador, Peru and Chile, coastal northwestern Africa, coastal southwestern Africa, and coastal northeastern Africa (Schubert *et al.*, 1979).

Because of their widespread global coverage and their impact on the global climate, it is no wonder that extensive modeling studies of marine stratocumulus clouds have been undertaken, the goals of which are to better understand the interaction of the variables

and processes which govern the formation, maintenance, and dissipation of these clouds. The difficulty in such modeling comes from the extensive parameterization of such complex physical processes as radiation, entrainment, and turbulent fluxes.

The first to develop a model of the cloud-topped marine boundary layer was Lilly (1968). His model emphasized longwave cooling off cloud top as the important driving mechanism for stratocumulus. This elegant, one-dimensional, mixed layer model was soon followed by several models which attempted to generalize his mixed layer theory (Schubert, 1976; Kraus and Schaller, 1978a; Schubert *et al.*, 1979). More complicated, higher-order models of the marine stratocumulus clouds have also been developed which are able to represent the marine boundary layer with significant success (e.g., Bougeault, 1985). However, the accuracy of the simpler, more computationally efficient mixed-layer models suggest that they will continue to play an important role in understanding the marine boundary layer. Randall (1985b) best described the importance of mixed layer models when he said, "Although complex models are capable of simulating many details of the cloud-topped marine boundary layer with remarkable accuracy, simple models continue to be of great importance, for reasons that go beyond their computational efficiency. It is often more challenging to represent a process in a simple model than in a complex one; the realistic incorporation of a process into a simple model marks the achievement of real understanding." For these reasons, we have chosen to study the marine boundary layer and the effect of the diurnal cycle with a simple one-dimensional mixed layer model.

The model presented here is a slight generalization of Lilly's (1968) mixed layer model. For this study, Lilly's (1968) model is generalized by considering both the net radiative flux divergence at cloud top as well as the net radiative flux divergence within the mixed layer to be important. We also allow the absorbed shortwave radiation to vary with the sun angle to enable us to simulate the diurnal cycle. In addition to these changes, Lilly's (1968) closure equation is slightly modified. We have chosen two closure assumptions for this study. The first closure is a weighted average of Lilly's (1968) maximum and minimum entrainment case. This method was first proposed by Schubert (1976). The second closure method considers the ratio of the integral buoyant energy dissipation to

the integral buoyant energy production to be constant. The models for both closure methods are presented for the steady state case as well as the time dependent case.

The outline of this paper is as follows. Chapter two is a review of Lilly's original mixed-layer model while chapter three describes the revisions and generalizations made to his model and the radiation parameterization. Experimental results of our models for both the steady-state and time dependent cases as well as the observational studies of Betts (1988) and Davies and Blaskovic (1988) are presented in chapter four. These experiments focus mainly on a comparison of the two closure assumptions and the simulation of the observed diurnal thinning of stratocumulus cloud decks. Finally, our conclusions are presented in chapter five.

Chapter 2

REVIEW OF LILLY'S CLOUD TOPPED MIXED LAYER MODEL

In a paper which has become a classic in the study of the marine boundary layer, Lilly (1968) presents two boundary layer models—one for the dry boundary layer case and one for the cloud-topped case. This chapter is devoted to reviewing the cloud-topped case of Lilly's paper.

Before looking at the mechanics of Lilly's model, it is first necessary to list the assumptions that are built in. The first assumption is that shear generated turbulence is confined to the lowest few tens of meters and can therefore be neglected. The radiation off the cloud top, however, is considered to be essential (Lilly, 1968) and strong enough to thoroughly mix the boundary layer through turbulent processes. Secondly, the air above the mixed layer (boundary layer) is assumed to be non-turbulent and of high enough temperature that if forced into the mixed layer, evaporative cooling would not lower its temperature beyond that of the mixed layer. If this happens, the air at cloud top would become negatively buoyant and penetrate freely into the mixed layer until the cloud was completely evaporated. For a change in mixing ratio across the inversion of 5–10 g/kg, an increase in potential temperature of $\sim 13 - 26°C$ is required for no change in temperature to occur upon evaporative mixing (Lilly, 1968). In more concise terms, Lilly's (1968) condition for a stable cloud layer is that the equivalent potential temperature of the air above the inversion must be at least as great as that of the air in the mixed layer. Thirdly, the mixed layer is assumed to be free of horizontal variations, i.e., it is assumed to be horizontally homogeneous. Finally, the large scale horizontal divergence and surface data are assumed to be known. With these assumptions in hand, Lilly's cloud-topped model can be derived.

For a layer in which no condensation takes place, the potential temperature (θ) and water vapor mixing ratio (q) can be regarded as conservative thermodynamic variables. In addition, if the layer is well mixed, θ and q can be regarded constant within the mixed layer. In a cloud topped mixed layer, θ and q are no longer appropriate conservative thermodynamic variables because condensation must now occur. However, if the resulting liquid water (ℓ) is not precipitated but rather is carried along with the air, the total water mixing ratio ($q + \ell$) and equivalent potential temperature (θ_e) can then be considered the appropriate conservative thermodynamic variables. Therefore, in a well mixed boundary layer of depth H, θ_e and $q + \ell$ remain constant in height. It should be noted that the omission of precipitation restricts the model to rather thin cloud layers.

Assuming the mixed layer is shallow compared to the scale height of the atmosphere, the thermodynamics can be simplified through the use of a linear condensation model. To derive this relationship, the Clausius-Clapeyron equation is combined with the hydrostatic equation. The result is a differential relationship between saturation mixing ratio, potential temperature, and height. This relationship is given by

$$dq_{sat} = ad\theta - bdz, \tag{2.1}$$

where

$$a = \frac{Lq_{sat}}{R_v T\theta}\left(\frac{p}{p - e_s}\right),$$

and

$$b = \frac{gpq_{sat}}{(p - e_s)\, c_p}\left(\frac{L}{R_v T^2} - \frac{c_p}{RT}\right)$$

(see Appendix for the complete derivation and definitions of terms). Although a and b are both rapidly changing functions of height, Lilly maintains that for a shallow layer they may be considered constant.

The shallow layer approximation can also be used to simplify our definition of θ_e. Lilly (1968) defines θ_e as a measure of the total sensible plus latent heat of the air. For a shallow layer where $T \approx \theta \approx \theta_e$, we can express θ_e as a differential relationship between potential temperature and water vapor mixing ratio. Specifically,

$$d\theta_e = d\theta + \frac{L}{c_p} dq. \tag{2.2}$$

With the use of (2.1) and (2.2), one can easily derive an expression for the cloud base height. This is done by integrating (2.1) upwards from the sea-surface to cloud base (h). Potential temperature can then be eliminated from the resulting expression through substitution of (2.2). The end result is

$$bh = (1+\alpha)[q_S - (q+\ell)] - a(\theta_{eS} - \theta_e) \tag{2.3}$$

where q_S and θ_{eS} are the saturation mixing ratio and saturation equivalent potential temperature at the sea surface, and $\alpha \equiv (aL/c_p)$ where L is latent heat and c_p is the specific heat of dry air at constant pressure. Here and throughout this paper, the subscript S will refer to those properties at the surface.

Again assuming that the boundary layer depth is much smaller than the scale height of the atmosphere, it can be shown that the vertical heat flux is a linear function of height. This is done by first combining the thermal equation, $d\theta_e/dt = 0$, with the Boussinesq form of the continuity equation to obtain the thermal equation in flux form. By imposing the assumption of horizontal homogeneity (i.e., $\partial\theta_e/\partial x = \partial\theta_e/\partial y = 0$) and the assumption that the boundary layer is well mixed in θ_e (i.e., $\partial\theta_e/\partial z = 0$) the thermal equation is reduced to

$$\frac{\partial\theta_e}{\partial t} = -\frac{\partial}{\partial z}(\overline{w'\theta_e'}). \tag{2.4}$$

Since θ_e is constant with height, it follows from (2.4) that $\overline{w'\theta_e'}$ is a linear function of height. This linear relationship can be expressed as

$$\overline{w'\theta_e'} = \left(1 - \frac{z}{H}\right)(\overline{w'\theta_e'})_S + \frac{z}{H}(\overline{w'\theta_e'})_H, \tag{2.5}$$

where the subscript H refers to those properties just below cloud top. By substituting (2.5) into (2.4), the thermal equation for the mixed layer is written in final form as

$$\frac{\partial\theta_e}{\partial t} = \frac{[(\overline{w'\theta_e'})_S - (\overline{w'\theta_e'})_H]}{H}. \tag{2.6}$$

By analogy, starting with $d(q+\ell)/dt = 0$, the total water mixing ratio equation for the mixed layer is written as

$$\frac{\partial(q+\ell)}{\partial t} = \frac{\overline{w'(q'+\ell')}_S - \overline{w'(q'+\ell')}_H}{H}. \tag{2.7}$$

At the upper boundary (cloud top), the thermal equation takes a different form. For cloud top, Lilly (1968) states that if a stable temperature discontinuity is to exist, it must be maintained by an infinite heating or cooling rate associated with a discontinuity in the radiative and/or turbulent heat fluxes. For this reason, the thermal equation at cloud top must now include both the vertical variation in θ_e and the radiative flux (F). With this in mind, the thermal equation at cloud top is written as

$$\frac{\partial \theta_e}{\partial t} = -w_H \frac{\partial \theta_e}{\partial z} - \frac{\partial}{\partial z}(\overline{w'\theta_e'}) - \frac{\partial F}{\partial z}. \tag{2.8}$$

If (2.8) is integrated from just below cloud base (H^-) to an equal distance just above cloud base (H^+) the following expression is obtained

$$\int_{H-}^{H^+} \frac{\partial \theta_e}{\partial t} dz = -w_H(\theta_{eU} - \theta_e) + (\overline{w'\theta_e'})_H - F_U \tag{2.9}$$

where the subscript U refers to those properties just above cloud top. However, (2.9) by can be simplified by first using Leibniz' rule to expand the left hand side, i.e.,

$$\int_{H-}^{H^+} \frac{\partial \theta_e}{\partial t} dz = \frac{\partial}{\partial t} \int_{H-}^{H^+} \theta_e dz - \frac{\partial H}{\partial t}(\theta_{eU} - \theta_e). \tag{2.10}$$

As we take the limit $\Delta H \rightarrow 0$, the first term on the right hand side vanishes, thus the heat balance equation at cloud top can be expressed as

$$\left(\frac{\partial H}{\partial t} - w_H\right) \Delta\theta_e + (\overline{w'\theta'})_H = F_U, \tag{2.11}$$

where $\Delta\theta_e \equiv \theta_{eU} - \theta_e$ and F_U is the net radiative cooling at cloud top. By analogy it can be shown that

$$\left(\frac{\partial H}{\partial t} - w_H\right) \Delta(q + \ell) + \overline{w'(q' + \ell')}_H = 0, \tag{2.12}$$

where $\Delta(q + \ell) = q_U - (q + \ell)$.

At the lower boundary (sea-surface), $\overline{w'\theta_e'}$ can be related to the near surface wind and the sea surface to air equivalent potential temperature difference through the use of a bulk transfer coefficient, C_T. By analogy, $\overline{w'(q' + \ell')}$ is related to the near surface wind and the sea surface to air water vapor mixing ratio difference. The resulting relationships are given as

$$(\overline{w'\theta_e'})_S = C_T V(\theta_{eS} - \theta_e) \tag{2.13}$$

and

$$\overline{w'(q'+\ell')}_S = C_T V[q_S - (q+\ell)]. \tag{2.14}$$

The wind speed, V, is typically measured from ten meters above the surface.

In order to close this system of equations, it is useful to discuss the concept of virtual potential temperature (θ_v). The virtual potential temperature is defined in the usual way as the potential temperature a parcel of air would have if it had the same density as dry air at the same pressure. It is therefore a measure of the relative buoyancy of the air. Lilly (1968) defines θ_v to include the contributions of both vapor and liquid water to the air density. Specifically,

$$d\theta_v = d\theta + \bar{\theta}(\delta dq - d\ell) \tag{2.15}$$

where $\delta \equiv [(1-\epsilon)/\epsilon]$ and ϵ is the ratio of the molecular weight of water to the molecular of dry air. The value of δ used here is 0.608. Since (2.2) and (2.15) are valid for both mean and fluctuating quantities, they can be expressed in terms of turbulent fluxes, i.e.,

$$\overline{w'\theta'_e} = \overline{w'\theta'} + \frac{L}{c_p}\overline{w'q'}, \tag{2.16}$$

$$\overline{w'\theta'_v} = \overline{w'\theta'} + \bar{\theta}(\delta\overline{w'q'} - \overline{w'\ell'}). \tag{2.17}$$

Using (2.16) and (2.17), the turbulent virtual potential temperature flux can be expressed in terms of more conservative quantities by eliminating the potential temperature flux between (2.16) and (2.17). The resulting expression is

$$\overline{w'\theta'_v} = \overline{w'\theta'_e} - \bar{\theta}\,\overline{w'(q'+\ell')} - \left[\frac{L}{c_p} - \bar{\theta}(\delta+1)\right]\overline{w'q'}. \tag{2.18}$$

Although (2.18) adequately describes the turbulent virtual potential temperature flux in the boundary layer, it is a discontinuous function across the cloud base because of the liquid water term. Beneath the cloud base, the liquid water vanishes allowing some cancellation between the third and fourth terms of (2.18). In the cloud, the mixing ratio becomes saturated, therefore (2.1) evaluated at constant height can be combined with (2.2) to show that

$$\overline{w'q'} = \frac{a}{(1+\alpha)}\overline{w'\theta'_e}. \tag{2.19}$$

Substituting (2.19) into (2.18) allows the second and fourth terms of (2.18) to be combined. Under these two conditions, (2.18) can be rewritten as

$$\overline{w'\theta'_v} = \begin{cases} \overline{w'\theta'_e} - \left(\frac{L}{c_p} - \bar{\theta}\delta\right)\overline{w'q'}, & \text{for } 0 < z < h; \\ \\ \frac{[1+a\bar{\delta}(\delta+1)]}{(1+\alpha)}\overline{w'\theta'_e} - \bar{\theta}\,\overline{w'(q'+\ell')}, & \text{for } h < z < H. \end{cases} \tag{2.20}$$

Having discussed the virtual potential temperature, it is now possible to return to the closure equation. Lilly (1968) proposes from considerations of the turbulent energy balance, that the equation necessary to close this system of equations is one which predicts the rate of turbulent entrainment. He offers two cases, one for the maximum entrainment case and one for the minimum entrainment case. These are

$$\text{Maximum}: \quad \int_0^H (\overline{w'\theta'_v})dz = 0, \quad \text{but} \quad \overline{w'\theta'_v} \neq 0 \quad \text{somewhere.} \tag{2.21}$$

$$\text{Minimum}: \quad (\overline{w'\theta'_v})_{\min} = 0, \quad \text{but} \int_0^H (\overline{w'\theta'_v})dz > 0. \tag{2.22}$$

The maximum entrainment case implies that the heat transported down from above the inversion equals that carried up from the surface. Viscous dissipation of energy is therefore neglected. The minimum case confines all the energy dissipation within the region of positive conversion from potential energy. No energy is transported to do work outside the boundaries of the positive conversion region (Lilly, 1968). Since viscous dissipation is sometimes large, observations show that the boundary layer tends more towards the minimum entrainment case (Lilly, 1968).

Chapter 3

MODELING THEORY

Presented in this chapter are both the time dependent and steady-state, horizontally homogeneous, cloud-topped mixed layer models based primarily on the work of Lilly (1968) and Schubert *et al.* (1979). The conservative thermodynamic variables are equivalent potential temperature θ_e and total water mixing ratio $q + \ell$. Some of the differences between these and Lilly's (1968) model are: (1) radiation is allowed to penetrate into the boundary layer; (2) cloud top values of longwave radiation, equivalent potential temperature, and water vapor mixing ratio are linear functions of height derived from climatological data for California coastal stations; (3) two closure assumptions are explored, the first assumes a weighted average of Lilly's (1968) maximum and minimum entrainment theories, the second assumes the ratio of the integral buoyant energy dissipation over the integral buoyant energy production is constant.

Section 3.1 describes in detail the revisions made to Lilly's (1968) model and the two closure assumptions. Section 3.2 decribes the radiation parameterization. Section 3.3 describes the combined radiative-convective model for both closure assumptions. Finally, section 3.4 discusses the steady-state solutions to the combined radiative-convective model, again for both closure assumptions.

3.1 REVISIONS TO LILLY'S MODEL

In Lilly's (1968) model, the radiation is confined to an infinitesimally thin layer at cloud top. Observational results from Slingo *et al.* (1982) and Albrecht *et al.* (1985), however, indicate that substantial radiative cooling occurs in the mixed layer. For this reason, the models presented in this chapter lift this restriction of longwave cooling to

cloud top and thus allow radiation to penetrate into the mixed layer. The immediate result of this assumption is the inclusion of the vertical variation of the radiative flux in the mixed layer thermal equation (2.4). The new mixed layer thermal equation is written as

$$\frac{\partial \theta_e}{\partial t} = -\frac{\partial}{\partial z}(\overline{w'\theta_e'}) - \frac{\partial F}{\partial z}, \tag{3.1}$$

where F is the radiative flux. Since θ_e is well mixed in the vertical, it follows from (3.1) that $(\overline{w'\theta_e'} + F)$ is a linear function of height. Further, if the radiative flux alone is assumed to be linear with height, then $\overline{w'\theta_e'}$ must also be linear with height. These linear relationships are given as

$$F = \left(1 - \frac{z}{H}\right) F_S + \frac{z}{H} F_H \tag{3.2}$$

and (2.5) respectively. By substituting (2.5) and (3.2) into (3.1), the mixed layer thermal equation becomes

$$\frac{\partial \theta_e}{\partial t} = \frac{(\overline{w'\theta_e'})_S - (\overline{w'\theta_e'})_H + F_S - F_H}{H}. \tag{3.3}$$

The cloud top thermal equation (2.11) is also slightly revised The new cloud top thermal equation takes the form

$$\left(\frac{\partial H}{\partial t} - w_H\right) \Delta\theta_e + (\overline{w'\theta_e'}) = F_U - F_H \tag{3.4}$$

As can be seen, (3.4) is the same as (2.11) with the exception that $F_U - F_H$ now represents the net radiative cooling at cloud top. This distinction is made for consistency with (3.3).

The second revision made to Lilly's (1968) model is in the calculation of the cloud top values of θ_e and q. Instead of holding these variables constant, they are allowed to vary linearly with height. The linear functions used in this model were derived from July averaged sounding data for San Diego and Oakland, CA taken from the *U.S. Dept. of Commerce Climatological Data, National Summary* for the years 1976–1980. These linear relationships are

$$q_U = \begin{cases} 5.50 - 0.00066 \times H, & \text{for San Diego;} \\ 5.54 - 0.00112 \times H, & \text{for Oakland} \end{cases} \tag{3.5}$$

and

$$\theta_{eU} = \begin{cases} 313.95 + 0.00566 \times H, & \text{for San Diego;} \\ 311.15 + 0.00341 \times H, & \text{for Oakland} \end{cases}, \tag{3.6}$$

where the units of q_U and θ_U are g kg^{-1} and Kelvin respectively.

A third revision to Lilly's (1968) model is the parameterization of the cloud top vertical velocity in terms of the large scale horizontal divergence. Because the vertical velocity at cloud top is difficult to measure, it is preferred to parameterize it in terms of a known climatological mean. In this case, the large scale horizontal divergence is used. The parameterization is accomplished by integrating the Bousinesq form of the continuity equation from the sea-surface to cloud top. Since the large scale horizontal divergence is constant with height in the boundary layer, the integration is simply

$$\left(\frac{\partial u}{\partial x}+\frac{\partial v}{\partial y}\right)\int_0^H dz = -\int_0^H \frac{\partial w}{\partial z}dz.$$

Carrying out the integration gives

$$-\left(\frac{\partial u}{\partial x}+\frac{\partial v}{\partial y}\right)H = w_H,$$

where $w(z=0)=0$ since the ocean surface is assumed to have no slope. By defining $D \equiv (\partial u/\partial x + \partial v/\partial y)$, (3.4) and (2.12) can be rewritten as

$$\left(\frac{\partial H}{\partial t}+DH\right)\Delta\theta_e + (\overline{w'\theta_e'})_H = F_U - F_H \tag{3.7}$$

and

$$\left(\frac{\partial H}{\partial t}+DH\right)\Delta(q+\ell) + \overline{w'(q'+\ell')}_H = 0, \tag{3.8}$$

Equations (3.7) and (3.8) are both predictive equations for H. In order that they predict H in a consistent manner,

$$\Delta(q+\ell)(\overline{w'\theta_e'})_H - \Delta\theta_e\ \overline{w'(q'+\ell')}_H = \Delta(q+\ell)(F_U - F_H). \tag{3.9}$$

Equation (3.9) is derived by multiplying (3.7) by $\Delta(q+\ell)$ and (3.8) by $-\Delta\theta_e$ and summing.

The revisions to Lilly's (1968) model are now complete with the exception of the closure equation. Two methods of deriving a closure equation are discussed in the following subsections. The first is taken from the work of Schubert (1976) where a weighted average of Lilly's (1968) maximum and minimum entrainment cases is considered. The second considers the ratio of the integral buoyant energy dissipation to the integral buoyant energy production to be constant, as suggested by Kraus and Schaller (1978b).

3.1.1 CLOSURE METHOD ONE

Schubert (1976) suggests that perhaps a better means of examining the marine boundary layer is to consider a weighted average of Lilly's maximum and minimum entrainment hypotheses. Using this concept, the closure equation takes the form

$$\frac{k}{H}\int_0^H \overline{w'\theta_v'}dz + (1-k)(\overline{w'\theta_v'})_{\min} = 0, \tag{3.10}$$

where $0 \leq k \leq 1$ and the equation for the turbulent virtual temperature flux is given by (2.20) and can be rewritten as

$$\overline{w'\theta_v'} = \begin{cases} \overline{w'\theta_e'} - \gamma\overline{w'(q'+\ell')}, & \text{for } 0 < z < h; \\ \\ \beta\overline{w'\theta_e'} - \bar{\theta}\,\overline{w'(q'+\ell')}, & \text{for } h < z < H. \end{cases} \tag{3.11}$$

where

$$\gamma \equiv \left(\frac{L}{c_p} - \bar{\theta}\delta\right) \quad \text{and} \quad \beta \equiv \frac{[1 + a\bar{\theta}(\delta+1)]}{(1+\alpha)}. \tag{3.12}$$

It should be mentioned that turbulent liquid water flux is zero for $0 < z < h$; however, it is included in (3.11) to simplify future derivations.

As mentioned previously, $\overline{w'\theta_e'}$ is linear with height throughout the mixed layer because θ_e is constant with height in the mixed layer. The same holds true for $\overline{w'(q'+\ell')}$ since $(q+\ell)$ is also constant with height in the mixed layer. This linear expression is analogous to (2.5) and is given as

$$\overline{w'(q'+\ell')} = \left(1 - \frac{z}{H}\right)\overline{w'(q'+\ell')}_S + \frac{z}{H}\overline{w'(q'+\ell')}_H \tag{3.13}$$

Because $\overline{w'\theta_e'}$ and $\overline{w'(q'+\ell')}$ are linear functions of height, it follows from (3.11) that $\overline{w'\theta_v'}$ must also be a linear in height but with a discontinuity across cloud base. One might think then that the minimum in $\overline{w'\theta_v'}$ could occur at one of four places, at the surface, just below cloud base, just above cloud base, or at cloud top. However, a closer examination of (3.11) shows that the jump in $\overline{w'\theta_v'}$ across cloud base must always be positive. This eliminates the possibility of a minimum in $\overline{w'\theta_v'}$ occurring just above cloud base since the value just below cloud base will always be less. To show this, use (3.11) to take the

difference between $(\overline{w'\theta'_v})_{h+}$ and $(\overline{w'\theta'_v})_{h-}$, where h^+ and h^- refer to a height just above and just below cloud base respectively. After some algebraic manipulation the result can be written as

$$(\overline{w'\theta'_v})_{h+} - (\overline{w'\theta'_v})_{h-} = \left(\bar{\theta}(\delta+1) - \frac{\alpha}{a}\right)\left(\frac{a}{1+\alpha}(\overline{w'\theta'_e})_h - \overline{w'(q'+\ell')}_h\right) \tag{3.14}$$

Because the air at cloud base is saturated, we can substitute (2.19) into (3.14). Making this substitution and cancelling terms gives

$$(\overline{w'\theta'_v})_{h+} - (\overline{w'\theta'_v})_{h-} = \left[\frac{\alpha}{a} - \bar{\theta}(\delta+1)\right](\overline{w'\ell'})_{h+} \tag{3.15}$$

Since $(\overline{w'\ell'})_{h+} > 0$, $(\alpha/a) > 0$, and $(\alpha/a) \gg \bar{\theta}(\delta+1)$, the left hand side of (3.15) must be positive. The only remaining possible locations for the minimum turbulent virtual potential temperature flux are at the surface, just below cloud base, or at cloud top.

Using the above constraints, the integrated closure equation can be derived by substituting (2.5), (3.11), and (3.13) into (3.10) and integrating. The resulting closure equation relates H, h, $(\overline{w'\theta'_e})_S$, $(\overline{w'\theta'_e})_H$, $\overline{w'(q'+\ell')}_S$, and $\overline{w'(q'+\ell')}_H$. This relationship is written as

$$\begin{aligned}
&\left\{\left[\frac{(1-\beta)}{H}\left(2h - \frac{h^2}{H}\right) + \beta\right](\overline{w'\theta'_e})_S + \left[(1-\beta)\left(\frac{h^2}{H^2}\right) + \beta\right](\overline{w'\theta'_e})_H\right. \\
&\left. - \left[\frac{(\gamma-\bar{\theta})}{H}\left(2h - \frac{h^2}{H}\right) + \bar{\theta}\right]\overline{w'(q'+\ell')}_S - \left[(\gamma-\bar{\theta})\left(\frac{h^2}{H^2}\right) + \bar{\theta}\right]\overline{w'(q'+\ell')}_H\right\} \\
&+ \frac{2(1-k)}{k} \times \text{ the minimum of} \\
&\left\{\begin{array}{c} \beta(\overline{w'\theta'_e})_H - \bar{\theta}\,\overline{w'(q'+\ell')}_H \\ \left(1-\frac{h}{H}\right)(\overline{w'\theta'_e})_S + \frac{h}{H}(\overline{w'\theta'_e})_H - \gamma\left(1-\frac{h}{H}\right)\overline{w'(q'+\ell')}_S - \gamma\frac{h}{H}\overline{w'(q'+\ell')}_H \\ (\overline{w'\theta'_e})_S - \gamma\,\overline{w'(q'+\ell')}_S \end{array}\right\} = 0
\end{aligned} \tag{3.16}$$

3.1.2 CLOSURE METHOD TWO

For closure method two, the ideas of Kraus and Schaller (1978b) are followed in that a closure equation which is based on the ratio of the integral buoyant energy dissipation over the integral buoyant energy production is considered, i.e.,

$$k\int_0^H [\overline{w'\theta'_v} > 0]dz + \int_0^H [\overline{w'\theta'_v} < 0]dz = 0. \tag{3.17}$$

As with closure method one however, the closure equation still varies with the shape of the virtual potential temperature flux profile. It is therefore assumed that $(\overline{w'\theta'_v})_H > 0$ and only the three profiles given in Fig. 3.1 are considered.

The first step in determining which virtual potential temperature flux profile to use is to check the sign of $(\overline{w'\theta'_v})_0$. If it is positive, Fig. 3.1a is the appropriate profile to use and the closure equation takes the form

$$k\left\{\left[(\overline{w'\theta'_v})_{h+} + (\overline{w'\theta'_v})_H\right](H-h) + z_c(\overline{w'\theta'_v})_S\right\} + (h-z_c)(\overline{w'\theta'_v})_{h-} = 0 \qquad (3.18)$$

where z_c is the crossover height at which $(\overline{w'\theta'_v}) = 0$ between the surface and cloud base. This crossover height is given by

$$\frac{z_c}{h} = \frac{(\overline{w'\theta'_v})_S}{(\overline{w'\theta'_v})_S - (\overline{w'\theta'_v})_{h-}} \qquad (3.19)$$

Equations (3.9), (3.18), and (3.19) form a nonlinear system of equations in the three unknowns z_c, $(\overline{w'\theta'_e})_H$, and $\overline{w'(q'+\ell')}_H$. A solution is found by algebraically reducing the system of equations to one quadratic equation in the unknown z_c and iteratively finding its zero using a simple secant algorithm.

If $(\overline{w'\theta'_v})_S \leq 0$, the closure equation can take on two different forms corresponding to Fig.s 3.1b and 3.1c. To determine a solution, it is first assumed that $(\overline{w'\theta'_v})_{h-} \leq 0$. Under this restriction, the closure takes the form

$$k\left[(\overline{w'\theta'_v})_{h+} + (\overline{w'\theta'_v})_H\right](H-h) + \left[(\overline{w'\theta'_v})_S + (\overline{w'\theta'_v})_{h-}\right]h = 0 \qquad (3.20)$$

Equations (3.9) and (3.20) form a linear system of two equations in the unknowns $(\overline{w'\theta'_e})_H$, and $\overline{w'(q'+\ell')}_H$ which can easily be solved algebraically. Once the solution is found, (3.11) may be used to determine if it fits the assumed $\overline{w'\theta'_v}$ profile shape. If it does not, the shape of the virtual potential temperature profile is assumed to be that of Fig. 3.1c. In this case, the closure equation takes the form

$$k\left\{(h-z_c)(\overline{w'\theta'_v})_{h-} + \left[(\overline{w'\theta'_v})_{h+} + (\overline{w'\theta'_v})_H\right](H-h)\right\} + (\overline{w'\theta'_v})_S z_c = 0 \qquad (3.21)$$

Equations (3.9), (3.19) and (3.21) can then be used to solve for $(\overline{w'\theta'_e})_H$ and $\overline{w'(q'+\ell')}_H$ in the same manner as for the case where $(\overline{w'\theta'_v})_S > 0$.

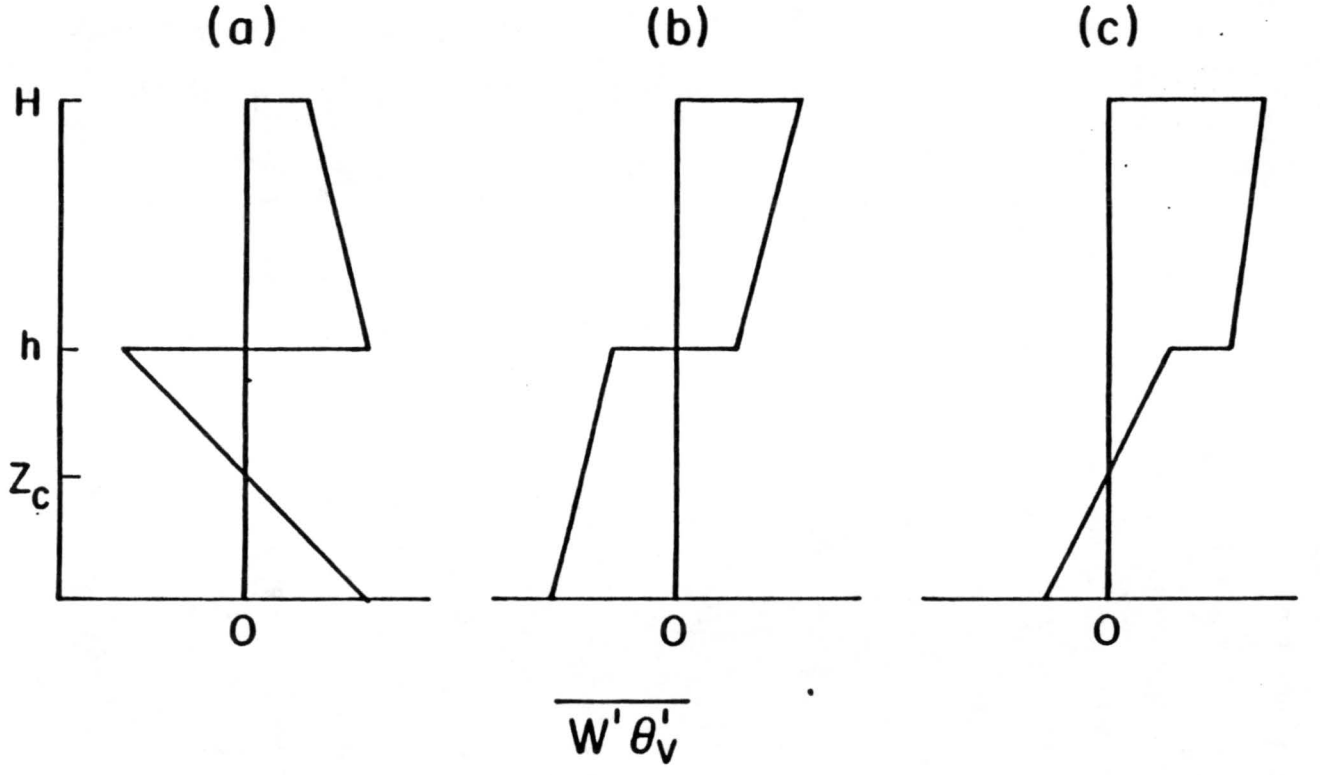

Figure 3.1: The shapes of the three possible profiles for the virtual potential temperature flux.

3.2 RADIATION PARAMETERIZATION

Since longwave cooling off cloud top is the important driving mechanism in the marine boundary layer, the radiation paramaterization warrants a detailed description. The philosophy that, consistent with the limitation of the vertical thermal structure to two degrees of freedom, the vertical resolution of the radiative cooling should also be limited to two degrees of freedom is followed. This means radiation can appear at most in both the mixed layer thermal equation (3.3) and the cloud top thermal equation (3.4). This is slightly different from Lilly's (1968) model where radiative cooling appears only in the cloud top thermal equation (2.11).

Schubert (1979) gives the equations for the net radiative flux as

$$F_U - F_H = (\rho c_p)^{-1}\{(1-\mu)(\sigma T_H^4 - \mathcal{L}_U^{\downarrow}) - (1-\mu')\mathcal{S}\}, \tag{3.22}$$

and

$$F_H - F_S = (\rho c_p)^{-1}\{\mu(\sigma T_H^4 - \mathcal{L}_U^{\downarrow}) - \mu'\mathcal{S}\}, \tag{3.23}$$

where ρ is the air density, σ is the Stefan-Boltzmann constant, T_H is the cloud top temperature in Kelvin, $\mathcal{L}_U^{\downarrow}$ is the downward longwave radiative flux in Wm^{-2} attributed to that portion of the atmosphere which lies above the mixed layer, $\mathcal{S}$ is the absorbed broadband shortwave radiative flux in Wm^{-2}, and μ and μ' are the longwave and shortwave radiation partitions respectively. These partitions can take on values from zero to one. If both are set to zero, the radiation parameterization reduces to Lilly's case.

For this model, the downward longwave radiative flux term in (3.22) and (3.23) is expressed as a linear function of cloud top height. The function was derived based on July averaged sounding data for the five years 1976–1980 as extracted from the *U.S. Dept. of Commerce Climatological Data, National Summary.* Two California locations were used, San Diego and Oakland. The sounding data combined with the midlatitude ozone profile as taken from the *U.S. Standard Atmosphere Table, 1976* and a uniform carbon dioxide profile of $.501\mathrm{g\,kg}^{-1}$ was entered into a broadband longwave radiation model described by Cox (1973). The model output was used to calculate the linear relationships for the

two locations which are strictly functions of cloud top height. The resulting equations are given as

$$\mathcal{L}_U^{\downarrow} = \begin{cases} 333.2 - 0.02980 \times H, & \text{for San Diego;} \\ 333.2 - 0.02799 \times H, & \text{for Oakland} \end{cases} \tag{3.24}$$

where $\mathcal{L}_U^{\downarrow}$ is in units of Wm^{-2}.

The calculation for $\mathcal{S}$ was made by entering the above sounding data into a broadband shortwave radiation model described by Manabe and Wetherald (1967). Since $\mathcal{S}$ varied little with height at the levels of typical marine stratocumulus cloud tops, it is considered to be constant in height. The $\mathcal{S}$ calculation is, however, allowed to vary with time. This allows for the inclusion of a diurnal cycle into the model. For simplicity, only solar orbital geometry is considered in calculating the diurnal cycle. In short, the $\mathcal{S}$ calculation is taken to be only a function of the cosine of the solar zenith angle. The dependence of upon $\mathcal{S}$ optical path length is neglected. Figure 3.2 shows the difference between $\mathcal{S}$ as calculated without consideration of the optical path dependence and $\mathcal{S}$ as calculated with consideration the optical path dependence. As can be seen, the accuracy gained is not warranted for the amount of complexity that must be added to include the optical path dependence. In addition, its inclusion would require additional degrees of freedom for the radiation parameterization, which as mentioned previously, is not desirable.

The constraint on $\mathcal{S}$ is that it reaches its climatological maximum at local solar noon and goes to zero at both sunrise and sunset. The maximum value for $\mathcal{S}$ (corresponding to local solar noon) used for this model was taken from the 900mb level of the broadband shortwave radiation model output. This value was then multiplied by a cloud shortwave absorption coefficient of 7%. This absorption coefficient corresponds to Lilly's (1968) value which was calculated from the observational results of Neiburger (1949). The calculated maximum values of $\mathcal{S}$ are

$$\mathcal{S}_{\max} = \begin{cases} 75.2, & \text{for San Diego;} \\ 73.5, & \text{for Oakland,} \end{cases} \tag{3.25}$$

where $\mathcal{S}_{\max}$ is in units of Wm^{-1}.

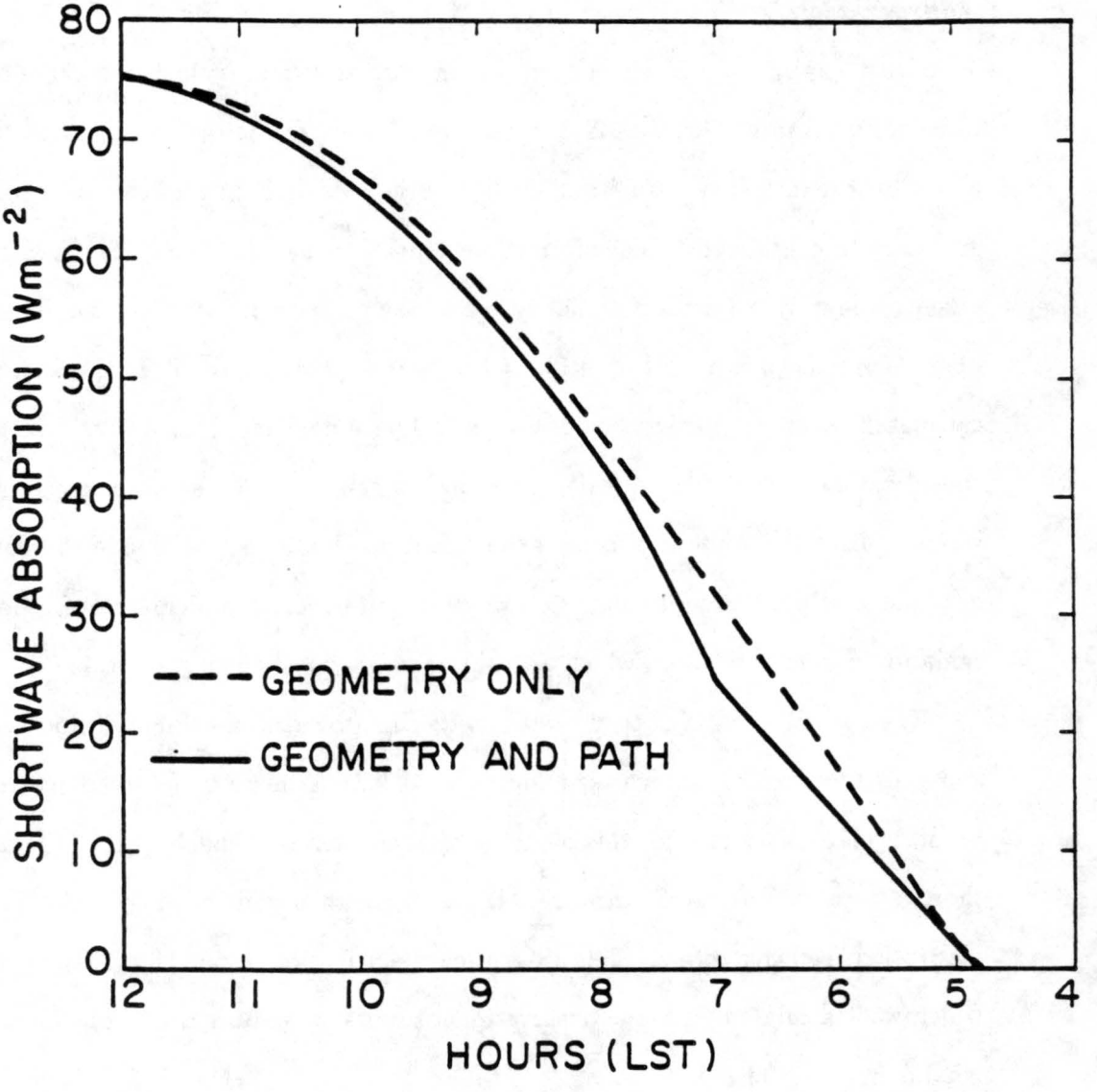

Figure 3.2: The absorbed broadband shortwave radiation. The dashed line represents calculations using solar geometry alone. The solid line represents calculations using both solar geometry and optical path dependence.

In summary, the equation for $\mathcal{S}$ is written as

$$\mathcal{S} = \mathcal{S}_0 \left(\frac{\bar{r}}{r}\right)^2 \{\sin\phi \sin d + \cos\phi \cos d \cos\tau\} \tag{3.26}$$

where ϕ is latitude, $\mathcal{S}_0$ is $\mathcal{S}_{\max}$ normalized by the local noon value of the cosine of solar zenith angle and the square of the distance function $(\bar{r}/r)$, $\bar{r}$ and r being, the mean and instantaneous distance of the earth from the sun respectively, d is the solar declination angle, and τ is the solar hour angle, i.e. the angular distance of a point on the earth from local solar noon. Note that the bracketed term in (3.26) is simply the definition of the cosine of the solar zenith angle. July averages for the calculations of r and d are based on data extracted from the *Smithsonian Meteorological Tables, 6th edition.*

Since $\mathcal{S}$, r, $\bar{r}$, ϕ, and d are constant with time (within the time frame of a few days), all time dependence in the shortwave radiation calculation must stem from the hour angle. This time dependence can be written as

$$\tau = \frac{\pi}{12}(t - 12), \tag{3.27}$$

where τ is in radians and t is the local sun time in hours.

In order to calculate the radiative terms $(F_U - F_H)$ and $(F_H - F_S)$, an equation for T_H is needed. This equation is derived first starting with the equation for potential temperature at cloud top (θ_H). The potential temperature at cloud top is equal to the potential temperature at cloud base (θ_h) plus the change that occurs when following a moist adiabat from cloud base to cloud top. That is

$$\theta_H = \theta_h + \left(\frac{\partial\theta}{\partial z}\right)_{\theta_e} (H - h). \tag{3.28}$$

However, $(\partial\theta/\partial z)_{\theta_e}$ is constant. To show this, simply set $d\theta_e = 0$ in (2.2) and substitute into (2.1). The result is

$$\left(\frac{\partial\theta}{\partial z}\right)_{\theta_e} = \frac{b}{a}\left(\frac{\alpha}{1+\alpha}\right). \tag{3.29}$$

In addition, θ_h can be calculated from our conservative thermodynamic variables by use of (2.2), i.e.,

$$\theta_h = \theta_e - \frac{L}{c_p}(q + \ell). \tag{3.30}$$

Substituting (3.29) and (3.30) into (3.28) while making use of Poisson's equation gives

$$T_H = \left[\theta_e - \frac{L}{c_p}(q+\ell) + C_1(H-h)\right]\left(\frac{p_H}{p_0}\right)^{\kappa} \tag{3.31}$$

where $C_1 \equiv (b/a)[\alpha/(1+\alpha)]$, p_0 is 1000 mb, p_H is the pressure at cloud top, and $\kappa \equiv (R/c_p)$ with R and c_p being, respectively, the ideal gas constant for dry air and the specific heat of dry air at constant pressure.

Equation (3.31) is not complete, however, since a way to calculate $(p_H/p_0)^{\kappa}$ is still needed. To do this, it is convenient to express the hydrostatic equation in terms potential temperature. The resulting expression is

$$dz = -\frac{c_p\theta}{g} d\left(\frac{p}{p_0}\right)^{\kappa}, \tag{3.32}$$

where g is gravity. By integrating (3.32) from the surface to cloud base, an expression for $(p_H/p_0)^{\kappa}$ can be derived. This integration, however, must be done in two steps since θ is constant below cloud base but is height dependent above cloud base.

The first step is to integrate from the surface to cloud base and the second step is to integrate from cloud base to cloud top. Integration of (3.32) from the surface to cloud base gives

$$\left[\left(\frac{p_S}{p_0}\right)^{\kappa} - \left(\frac{p_h}{p_0}\right)^{\kappa}\right] = \frac{gh}{c_p\theta_h}. \tag{3.33}$$

The integration of (3.32) from cloud base to cloud top, however, is slightly more difficult because of the height dependence of θ. The equation for $\theta(z)$ to use in this case is a more general form of (3.28). That is

$$\theta(z) = \theta_h + C_1(z-h). \tag{3.34}$$

Substituting (3.34) into (3.32) and integrating from cloud base to cloud top gives

$$\left[\left(\frac{p_h}{p_0}\right)^{\kappa} - \left(\frac{p_H}{p_0}\right)^{\kappa}\right] = \frac{g}{C_1 c_p}\ln\left(1 + \frac{C_1(H-h)}{\theta_h}\right). \tag{3.35}$$

By summing (3.33) with (3.35) we obtain the desired expression for $(p_H/p_0)^{\kappa}$, i.e.,

$$\left(\frac{p_H}{p_0}\right)^{\kappa} = \left(\frac{p_S}{p_0}\right)^{\kappa} - \frac{gh}{c_p\theta_h} - \frac{g}{C_1 c_p}\ln\left(1 + \frac{C_1(H-h)}{\theta_h}\right). \tag{3.36}$$

By substituting (3.36) into (3.31), T_H can be expressed in terms of predicted model variables and known constants. This expression takes the form

$$T_H = [\theta_h + C_1(H-h)]\left\{\left(\frac{p_S}{p_0}\right)^{\kappa} - \frac{gh}{c_p\theta_h} - \frac{g}{c_pC_1}\ln\left(1+\frac{C_1(H-h)}{\theta_h}\right)\right\}. \qquad (3.37)$$

In summary, with the use of (3.24), (3.26), and (3.37), the radiation variables $F_U - F_H$ and $F_H - F_S$ can be expressed completely in terms of predicted model variables and known constants.

3.3 THE COMBINED CONVECTIVE-RADIATIVE MODEL

With the revisions to Lilly's (1968) model complete as well as the radiation parameterization, a combined convective-radiative model for both closure methods can now be written. These two models are presented in the following two subsections.

3.3.1 CLOSURE METHOD ONE

Closure method one again corresponds to the weighted average of Lilly's maximum and minimum entrainment assumption. The model equations consist of the surface flux equations (2.13) and (2.14), the cloud base equation (2.3), the cloud top jump definitions as defined in (2.11) and (2.12), the cloud top temperature equation (3.37), the radiation equations (3.22) and (3.23), the consistency relation (3.9), the mixed layer thermal and total water budget equations (3.3) and (2.7) respectively, the cloud top thermal equation (3.4), and the closure equation (3.16). These thirteen equations form a closed set in thirteen unknowns. Since the model contains three predictive variables (θ_e, $(q+\ell)$, and H), three initial conditions are needed to start the model. It should be noted that any reasonable initial conditions of the predictive variables may be used as long as the model is run long enough for all variables to begin to repeat themselves. For the sake of computational efficiency, however, the initial conditions are obtained from the steady state solutions (which will be discussed in the following section). This assures the user of a rapid convergence to the real solution.

With the initial conditions specified, the numerical time integration is performed in the following order:

$$(\overline{w'\theta'_e})_S = C_T V(\theta_{eS} - \theta_e) \tag{3.38}$$

$$\overline{w'(q' + \ell')_S} = C_T V[q_S - (q + \ell)] \tag{3.39}$$

$$h = \frac{(1+\alpha)[q_S - (q+\ell)] - a(\theta_{eS} - \theta_e)}{b} \tag{3.40}$$

$$\Delta\theta_e = \theta_{eU} - \theta_e \tag{3.41}$$

$$\Delta(q + \ell) = q_U - (q + \ell) \tag{3.42}$$

$$T_H = [\theta_h + C_1(H-h)]\left\{\left(\frac{p_S}{p_0}\right)^{\kappa} - \frac{gh}{c_p\theta_h} - \frac{g}{c_p C_1}\ln\left(1 + \frac{C_1(H-h)}{\theta_h}\right)\right\}, \tag{3.43}$$

$$F_U - F_H = (\rho c_p)^{-1}\{(1-\mu)(\sigma T_H^4 - \mathcal{L}_U^{\downarrow}) - (1-\mu')\mathcal{S}\}, \tag{3.44}$$

$$F_H - F_S = (\rho c_p)^{-1}\{\mu(\sigma T_H^4 - \mathcal{L}_U^{\downarrow}) - \mu'\mathcal{S}\}, \tag{3.45}$$

$$\begin{bmatrix} a_{11} & a_{12} \\ a_{21} & a_{22} \end{bmatrix}\begin{bmatrix} (\overline{w'\theta'_e})_H \\ \bar{\theta}\,\overline{w'(q'+\ell')}_H \end{bmatrix} = \begin{bmatrix} b_1 \\ b_2 \end{bmatrix} \tag{3.46, 3.47}$$

$$\frac{\partial\theta_e}{\partial t} = \frac{(\overline{w'\theta'_e})_S - (\overline{w'\theta'_e})_H + F_S - F_H}{H} \tag{3.48}$$

$$\frac{\partial(q+\ell)}{\partial t} = \frac{(\overline{w'q'})_S - \overline{w'(q'+\ell')}_H}{H} \tag{3.49}$$

$$\frac{\partial H}{\partial t} = \frac{F_U - F_H - (\overline{w'\theta'_e})_H}{\Delta\theta_e} - DH \tag{3.50}$$

With the exception of (3.46) and (3.47), all the above equations are taken directly from previous text. These two equations are simply a shorthand matrix notation for (3.9) and (3.16). The dependent variables, externally specified parameters and constants for the above equations are given in Tables 3.1–3.4. For those values which depend on a reference temperature and/or pressure, we use sea-surface temperature minus 3.5 degrees and surface pressure minus 35 mb. This represents an approximate midpoint to the boundary layer.

The numerical time integration is best demonstrated by the following six step iteration process. These six steps constitute a single iteration cycle and are as follows:

1) Use the initial conditions of the predictive variables to calculate the surface fluxes $(\overline{w'\theta'_e})_S$ and $\overline{w'(q'+\ell')}_S$ using (3.38) and (3.39).

2) Calculate the cloud base height, h, using (3.40).

3) Calculate the cloud-top jumps in equivalent potential temperature and total water mixing ratio using (3.41) and (3.42).

4) Calculate the cloud-top temperature using (3.43). Using this value of T_H, calculate the radiative flux divergences using (3.44) and (3.45).

5) Using the two-by-two matrix given by (3.46) and (3.47), calculate cloud top fluxes $(\overline{w'\theta'_e})_H$ and $\overline{w'(q'+\ell')}_H$.

6) Integrate (3.48)–(3.50) using a classical fourth order Runge-Kutta scheme to predict new values of θ_e, $(q+\ell)$, and H. When completed, return to step one.

The above six step iteration is all straightforward with the exception of step five. Because of the form of (3.16), the minimum in $\overline{w'\theta'_v}$ must be known before the proper coefficient matrix and the column vector on the right hand side of (3.46) and (3.47) can be obtained. This, however, requires that variables we are trying to calculate, $(\overline{w'\theta_e})_H$ and $\overline{w'(q'+\ell')}_H$, be known. To avoid this circular reasoning, the minimum in $\overline{w'\theta'_v}$ is assumed to occur just below cloud base and both $(\overline{w'\theta'_e})_H$ and $\overline{w'(q'+\ell')}_H$ are then calculated. Equation (3.11) can then be used to determine if the minimum in $\overline{w'\theta'_v}$ actually did occur just below cloud base. If so, the correct solution has been found. If not, the minimum is

Table 3.1: Dependent Variables

H	cloud-top height
h	cloud-base height
θ_e	mixed layer equivalent potential temperature
$q + l$	mixed layer total water mixing ratio
$\overline{(w'\theta'_e)}_S$	surface equivalent potential temperature flux
$\overline{(w'\theta'_e)}_H$	cloud-top equivalent potential temperature flux
$\overline{w'(q' + l')}_S$	surface total water flux
$\overline{w'(q' + l')}_H$	cloud-top total water flux
$\overline{(w'\theta'_v)}_S$	virtual potential temperature flux at the surface
$\overline{(w'\theta'_v)}_{h-}$	virtual potential temperature flux just below cloud base
$\overline{(w'\theta'_v)}_{h+}$	virtual potential temperature flux just above cloud base
$\overline{(w'\theta'_v)}_H$	virtual potential temperature flux at cloud top
$\Delta\theta_e$	cloud top equivalent potential temperature jump
$\Delta(q + l)$	cloud top total water jump
T_H	cloud top temperature
$F_U - F_H$	cloud top radiative flux divergence
$F_H - F_S$	mixed layer radiative flux divergence

Table 3.2: Externally Specified Parameters

D	large-scale divergence
V	wind speed
θ_{eS}	equivalent potential temperature at sea surface temperature and pressure
q_S	saturation mixing ratio at sea surface temperature and pressure
θ_{eU}	equivalent potential temperature just above cloud top
q_U	total water mixing ratio just above cloud top
$\mathcal{L}\overset{\downarrow}{U}$	downward longwave radiation flux just above cloud top
$\mathcal{S}$	total shortwave radiation absorption
μ	longwave radiation partition
μ'	shortwave radiation partition
k	entrainment parameter

Table 3.3: Constants

c_p	specific heat at constant pressure
C_T	bulk transfer coefficient
g	gravity
σ	Stefan-Boltzman constant
δ	see (2.15)

Table 3.4: Constants which depend on reference temperature and/or pressure

ρ	density
β	see (3.12)
γ	see (3.12)
a	see (2.1)
b	see (2.1)
$\bar{\theta}$	reference potential temperature
C_1	see (3.31)
L	latent heat of condensation

assumed to occur at the surface and the above procedure is repeated. If no true minimum has yet been found, the procedure is repeated for a minimum at cloud top. If one and only one solution leads to no contradiction, the true solution is assumed to have been found.

This model has been programmed in FORTRAN and will run interactively on an IBM-compatible personal computer. This particular version of the program is titled STRATUS Version 2.0. STRATUS 2.0 allows the user to specify the sea-surface temperature, the large scale horizontal divergence, the wind speed, the entrainment parameter, the short-wave partition, the long wave partition, and the geographical location (San Diego, CA or Oakland, CA). Output for the tenth model day is then written to two data files, STRATUS.DAT and FLUXES.DAT. STRATUS.DAT contains a time series of the mixed layer equivalent potential temperature, the mixed layer total water mixing ratio, cloud base, cloud top, and a flag indicating the location of the minimum of the virtual potential temperature flux. FLUXES.DAT contains a time series of the equivalent potential temperature flux and the total water mixing ratio flux at both cloud top and the surface, and the radiative flux divergence at both cloud top and in the mixed layer.

3.3.2 CLOSURE METHOD TWO

As before, closure method two assumes the ratio of the integral buoyant energy dissipation to the integral buoyant energy production is a constant. This difference affects only equations (3.46) and (3.47). All other equations remain the same as in closure method one. Similarly, the numerical time integration is also identical to that of closure method one with the exception that step five now follows the iterative process discussed in section 3.1.2.

This model has also been programmed in FORTRAN and will run interactively on any IBM-compatible personal computer. The program is again titled STRATUS but with a version number of 2.1. The input and output of versions 2.0 and 2.1 are the same with the exception of the flag in STRATUS.DAT. This flag no longer indicates where the minimum in the virtual potential temperature flux is located, instead it indicates the shape of virtual potential temperature flux profile. It should be noted that if the solutions

for $(\overline{w'\theta'_e})_H$ and $\overline{w'(q'+\ell')}_H$ do not agree with any of the three profile shapes given in Fig. 3.1, the program will print an error message and abort. So far this problem has not been encountered for physically reasonable input data.

3.4 THE STEADY-STATE SOLUTIONS

Solving the model for the steady-state case is obviously much different than for the time dependent case. For the steady-state case, all derivatives with respect to time are set to zero and a system of nonlinear albebraic equations is obtained. The method used to solve for the steady-state case is to reduce the system of equations down to one equation in H and use a simple secant method algorithm to find its zero. Presented here are the steady state solutions for both closure methods.

Before describing the steady-state model equations, two items must be discussed. First, the diurnal cycle can no longer be defined for the steady-state case. Instead a daily averaged solar radiative flux ($\mathcal{S}$) value of 22.3 Wm^{-2} as suggested by Lilly (1968) will be used. This value corresponds to approximately 1.5 hours after sunrise or 1.5 hours before sunset (0615 hrs and 1745 hrs local sun time respectively). Second, from (3.49) we can see directly that under steady-state conditions, the total water flux, $\overline{w'(q'+\ell')}$, is constant with height. For this reason, all subscripts on this variable are dropped. With these two thoughts in mind, the derivation of the steady state solutions can now be presented.

The steady-state solutions are begun by first deriving expressions for the surface flux of equivalent potential temperature and total water flux in terms of constants and externally specified parameters (see Tables 3.2–3.4). The former is accomplished by eliminating the dependent variables θ_e and $(\overline{w'\theta'_e})_H$ between the steady-state forms of (3.38), (3.48) and (3.50). The resulting expression is

$$(\overline{w'\theta'_e})_S = \frac{(F_U - F_H) - (F_S - F_H) - DH(\theta_{eU} - \theta_{eS})}{\left(1 + \frac{DH}{C_T V}\right)}. \tag{3.51}$$

The latter expression can be derived by eliminating $(q + \ell)$ and $\overline{w'(q' + \ell')}_H$ between equations (3.8), (3.39), and (3.49). This expression is given as

$$\overline{w'(q' + \ell')} = \frac{DH(q_S - q_U)}{\left(1 + \frac{DH}{C_T V}\right)}. \tag{3.52}$$

The mixed layer equivalent potential temperature can also be eliminated from our cloud base equation. This is accomplished by substituting (3.38) and (3.39) into (3.40). The resulting expression is

$$h = \frac{(1 + \alpha)\overline{w'(q' + \ell')} - a(\overline{w'\theta'_e})_S}{bC_T V} \tag{3.53}$$

To derive an expression for $(\overline{w'\theta'_e})_H$, θ_e is eliminated from (3.50) by substituting in (3.38). This equation is

$$(\overline{w'\theta'_e})_H = (F_U - F_H) - \frac{DH}{C_T V}(\overline{w'\theta'_e})_S - DH(\theta_{eU} - \theta_{eS}) \tag{3.54}$$

All the necessary information is now available to calculate the virtual potential temperature flux at the surface, just below cloud base, just above cloud base, and at cloud top. These expressions are taken directly from (3.11) and are given respectively as

$$(\overline{w'\theta'_v})_S = (\overline{w'\theta'_e})_S - \gamma\overline{w'(q' + \ell')}, \tag{3.55}$$

$$(\overline{w'\theta'_v})_{h-} = (\overline{w'\theta'_e})_h - \gamma\overline{w'(q' + \ell')}, \tag{3.56}$$

$$(\overline{w'\theta'_v})_{h+} = \beta(\overline{w'\theta'_e})_h - \bar{\theta}\,\overline{w'(q' + \ell')}, \tag{3.57}$$

$$(\overline{w'\theta'_v})_H = \beta(\overline{w'\theta'_e})_H - \bar{\theta}\,\overline{w'(q' + \ell')}, \tag{3.58}$$

where $(\overline{w'\theta'_e})_h$ is defined using (2.5) as

$$(\overline{w'\theta'_e})_h = \left(1 - \frac{h}{H}\right)(\overline{w'\theta'_e})_S + \frac{h}{H}(\overline{w'\theta'_e})_H. \tag{3.59}$$

The importance of equations (3.55)–(3.59) will become apparent in the following two subsections.

3.4.1 CLOSURE METHOD ONE

As before, closure method one corresponds to a weighted average of Lilly's (1968) maximum and minimum entrainment case. The closure equation for this case is derived by simply integrating (3.10). This integration is easily accomplished since $\overline{w'\theta_v'}$ is linear with height. The difficulty stems from not knowing the location of $(\overline{w'\theta_v'})_{\min}$. Therefore, to solve this problem, it is assumed that $(\overline{w'\theta_v'})_{\min}$ is located just below cloud base. Under this restriction, the closure equation then takes the form

$$\frac{2(1-k)}{k}(\overline{w'\theta_v'})_{h-}+(\overline{w'\theta_v'})_H+(\overline{w'\theta_v'})_{h+}+\frac{h}{H}[(\overline{w'\theta_v'})_S+(\overline{w'\theta_v'})_{h-}-(\overline{w'\theta_v'})_H-(\overline{w'\theta_v'})_{h+}]=0. \tag{3.60}$$

Since all the variables except H are known, (3.60) can be solved using a simple secant method algorithm. Once the solution is found, it must be checked to determine if the minimum did actually occur just below cloud base. If it does, the solution is accepted. If it does not, $(\overline{w'\theta_v'})_{\min}$ is assumed to be located at the surface and H is solved for using the following closure equation.

$$\frac{2(1-k)}{k}(\overline{w'\theta_v'})_S+(\overline{w'\theta_v'})_H+(\overline{w'\theta_v'})_{h+}+\frac{h}{H}[(\overline{w'\theta_v'})_S+(\overline{w'\theta_v'})_{h-}-(\overline{w'\theta_v'})_H-(\overline{w'\theta_v'})_{h+}]=0. \tag{3.61}$$

Again the solution is checked to determine if the closure assumption is correct. If it is, the solution is accepted. If not, it is assumed that no solution exists. It should be noted that the possibility of $(\overline{w'\theta_v'})_{\min}$ occurring at cloud top has been neglected. It is seen from (3.54) and (3.58) that for this case to occur, the radiative cooling at cloud top would have to be negligible. Since radiative cooling is the primary driving mechanism for this model, it is unlikely that this case could physically occur.

With the closure equation determined, a closed set of equations (3.43)–(3.45) and (3.51)–(3.61) in the unknowns H, h, T_H, (F_U-F_H), (F_H-F_S), $(\overline{w'\theta_e'})_H$, $(\overline{w'\theta_e'})_h$, $(\overline{w'\theta_e'})_S$, $\overline{w'(q'+\ell')}$, $(\overline{w'\theta_v'})_H$, $(\overline{w'\theta_v'})_{h+}$, $(\overline{w'\theta_v'})_{h-}$, and $(\overline{w'\theta_v'})_S$ is obtained. The solution process can best be explained by the following four step iteration sequence.

1) Make an initial guess of the cloud top height H and the radiative flux divergences (F_U-F_H) and (F_H-F_S).

2) With the above initial guesses, use (3.51)–(3.59) to calculate in order $(\overline{w'\theta'_e})_S$, $\overline{w'(q'+\ell')}$, h, $(\overline{w'\theta'_e})_H$, $(\overline{w'\theta'_v})_S$, $(\overline{w'\theta'_v})_{h-}$, $(\overline{w'\theta'_v})_{h+}$, and $(\overline{w'\theta'_v})_H$. In addition, calculate the radiation variables T_H, $(F_U - F_H)$, and $(F_H - F_S)$ using (3.43)–(3.45).

3) Using the above information, check to see if (3.60) is satisfied within some tolerable limit. If it is not, use the secant method to predict a new H and return to step one until (3.60) is satisfied.

4) Once a solution has been found, check to see if $(\overline{w'\theta'_v})_{\min}$ occurs at the assumed location. If it does, the solution has been found. If it does not, repeat steps 1–3 substituting (3.61) in for (3.60).

This model has been programmed in FORTRAN and will run interactively on any IBM-compatible personal computer. The program, STRATUS Version 1.0, requires the following input: sea-surface temperature, large scale horizontal divergence, surface wind speed, longwave and shortwave radiation partitions, the entrainment parameter, the geographic location, and the initial guess for cloud top. Output consists of a table printed to screen containing values of the mixed layer equivalent potential temperature, mixed layer total water mixing ratio, the convective total water flux, the equivalent potential temperature flux at cloud top and the surface , the virtual potential temperature flux at cloud top, just above cloud base, just below cloud base, and at the surface, the radiative flux divergence at cloud top and in the mixed layer, the temperature at cloud top, the cloud top height, and the cloud base height.

3.4.2 CLOSURE METHOD TWO

As before, closure method two is based on the idea that the ratio of the integral buoyant energy dissipation over the integral energy production is constant. As with closure method one, the possibility of multiple closure equations based on different virtual potential temperature flux profiles still exists. Therefore, a similar procedure to that of closure method one is used. The profile shape is assumed to be that of Fig. 3.1a and (3.18) is used as our closure equation. Once the solution has been found, it is checked to see if it satisfies the assumed profile shape. If they match, the true solution is assumed to have

been found. If not, the profile shape is assumed to be that of of Fig. 3.1b and (3.20) is used as our closure equation. The above procedure is then repeated (if necessary) for the final profile shape using (3.21) as the closure equation. If one and only one solution leads to no contradiction, it is assumed to be the true solution. Note that similar to closure method one where the possibility of $(\overline{w'\theta_v'})_{\min}$ occurring at cloud top was not considered, the case where $(\overline{w'\theta_v'})_H < 0$ is not considered. This is neglected for the same reasons, it adds unnecessary complications to the program without providing any physically realistic solutions.

With our closure complete, the same four step iterative process described in section 3.4.1 can be followed. The only difference is that (3.18), (3.20) and (3.21) now replace (3.60) and (3.61).

This model has also been program in FORTRAN and will run interactively on any IBM-compatible computer. The program, STRATUS Version 1.1, requires the same input and produces the same output as version 1.0.

Chapter 4

EXPERIMENTS AND RESULTS

In this chapter the results of numerous experiments accomplished using STRATUS Versions 1.0, 1.1, 2.0, and 2.1 are presented. Section 4.1 discusses the experimental results from the steady-state models (STRATUS Versions 1.0 and 1.1), while section 4.2 discusses the experimental results from the time-dependent models (STRATUS Versions 2.0 and 2.1).

4.1 STEADY-STATE MODEL EXPERIMENTS AND RESULTS

Experimental results for the steady-state case are similar to the results of Schubert *et al.* (1979) obtained for similar input data. The purpose of this section is to examine the experimental results over a wider range in the shortwave radiation partition, μ'. Schubert *et al.* (1979) allowed μ' to vary in the range $0.0 \leq \mu' \leq 0.2$. Here, μ' is allowed to take on values as large as 1.0. The effects of this change are examined for both closure methods. Also examined are the effects of varying the divergence and sea-surface temperature on cloud top and base heights for both closure methods.

To examine the effects of varying the shortwave partition, cloud top, cloud base, and all convective fluxes have all been plotted as a function of μ' where $0 \leq \mu' \leq 1$, while holding the following parameters constant at the specified values: sea-surface temperature (16 °C), large scale horizontal divergence (5×10^{-6} s^{-1}), longwave radiation partition (0.2), the entrainment parameter (0.2), and the location (San Diego, CA) for both closure methods (Figs. 4.1–4.4). Figures 4.1 and 4.2 show the cloud top and base height curves for both closure methods. The results of these curves are as one might expect. As the shortwave partition is increased, more radiative cooling occurs at cloud top and, as a result, the

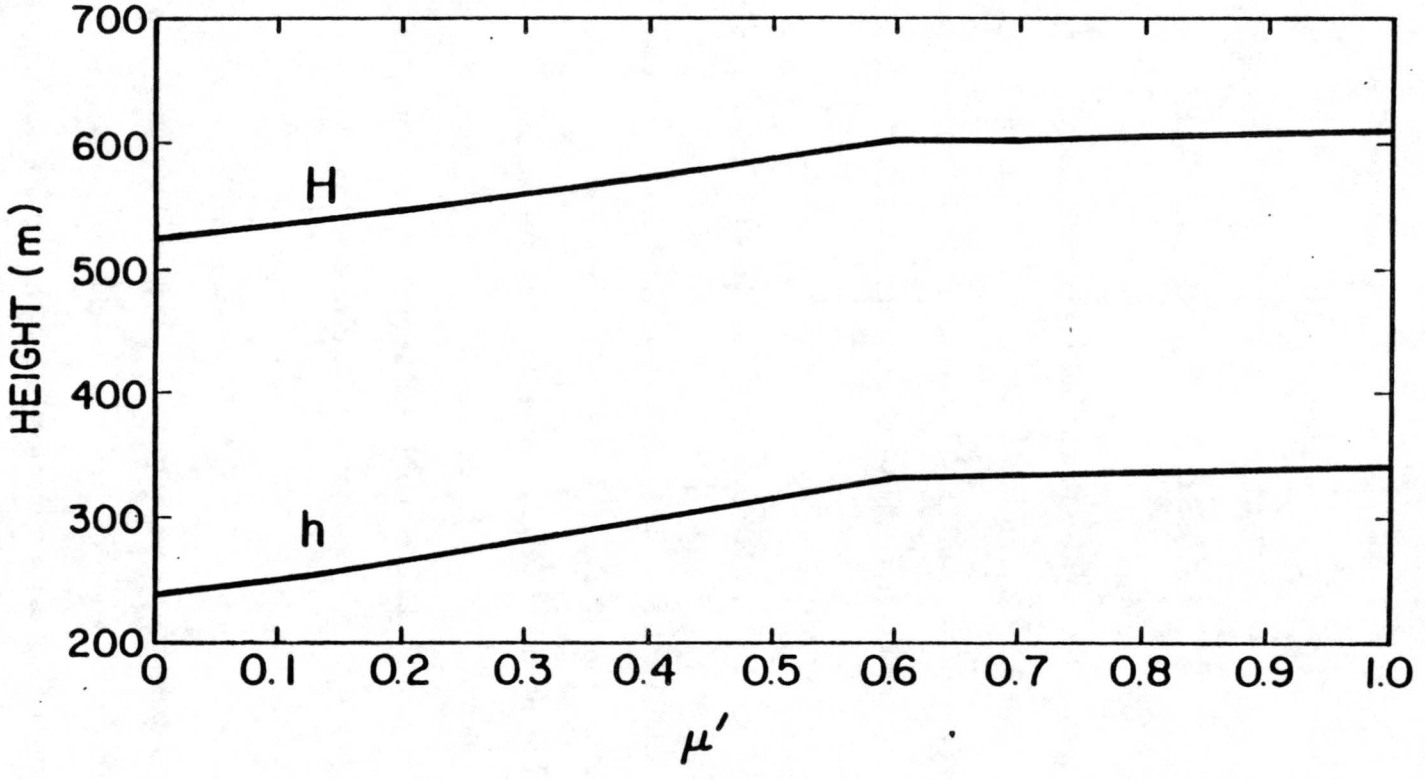

Figure 4.1: Steady-state values of cloud top and base height as a function of the shortwave partition, μ', for closure method one.

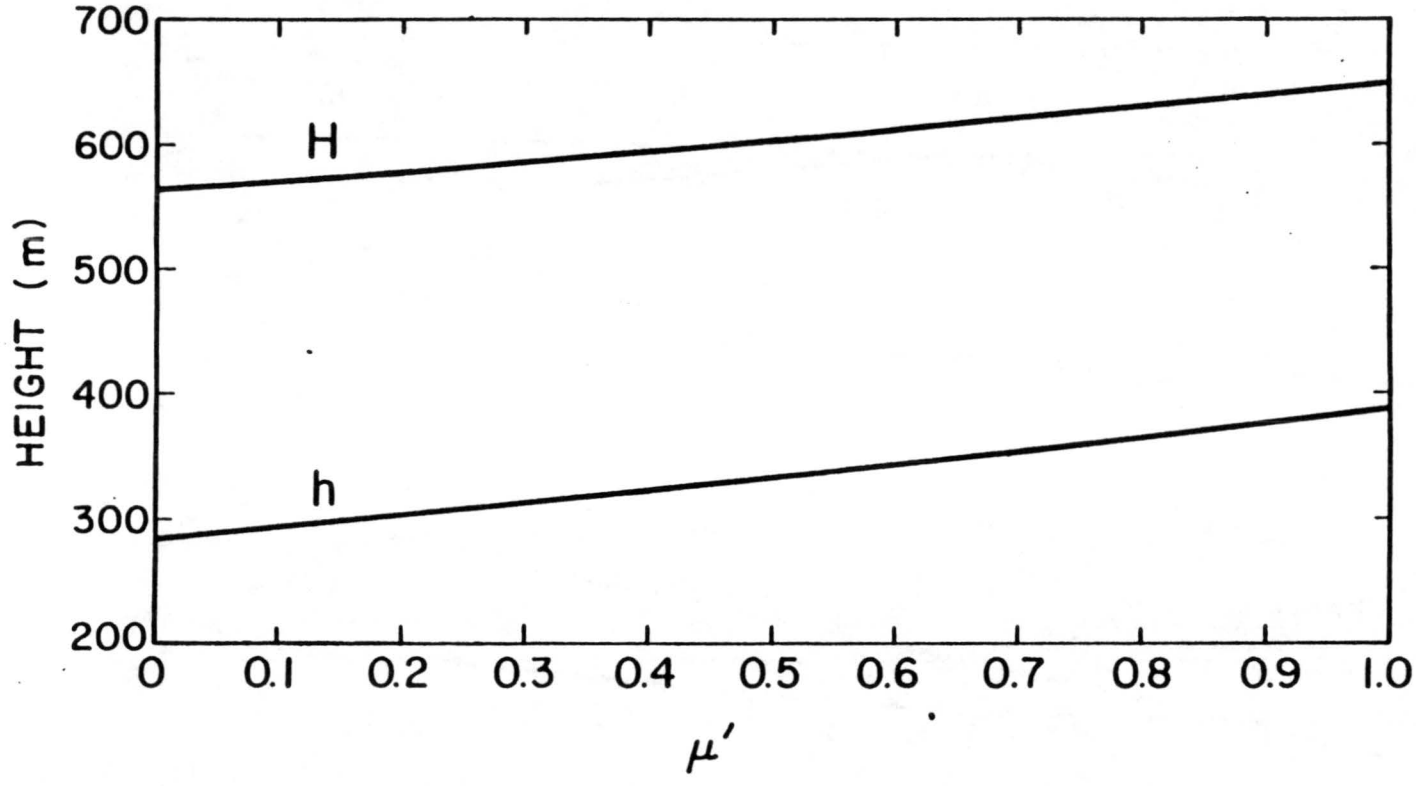

Figure 4.2: Steady-state values of cloud base and height as a function of the shortwave partition, μ', for closure method two.

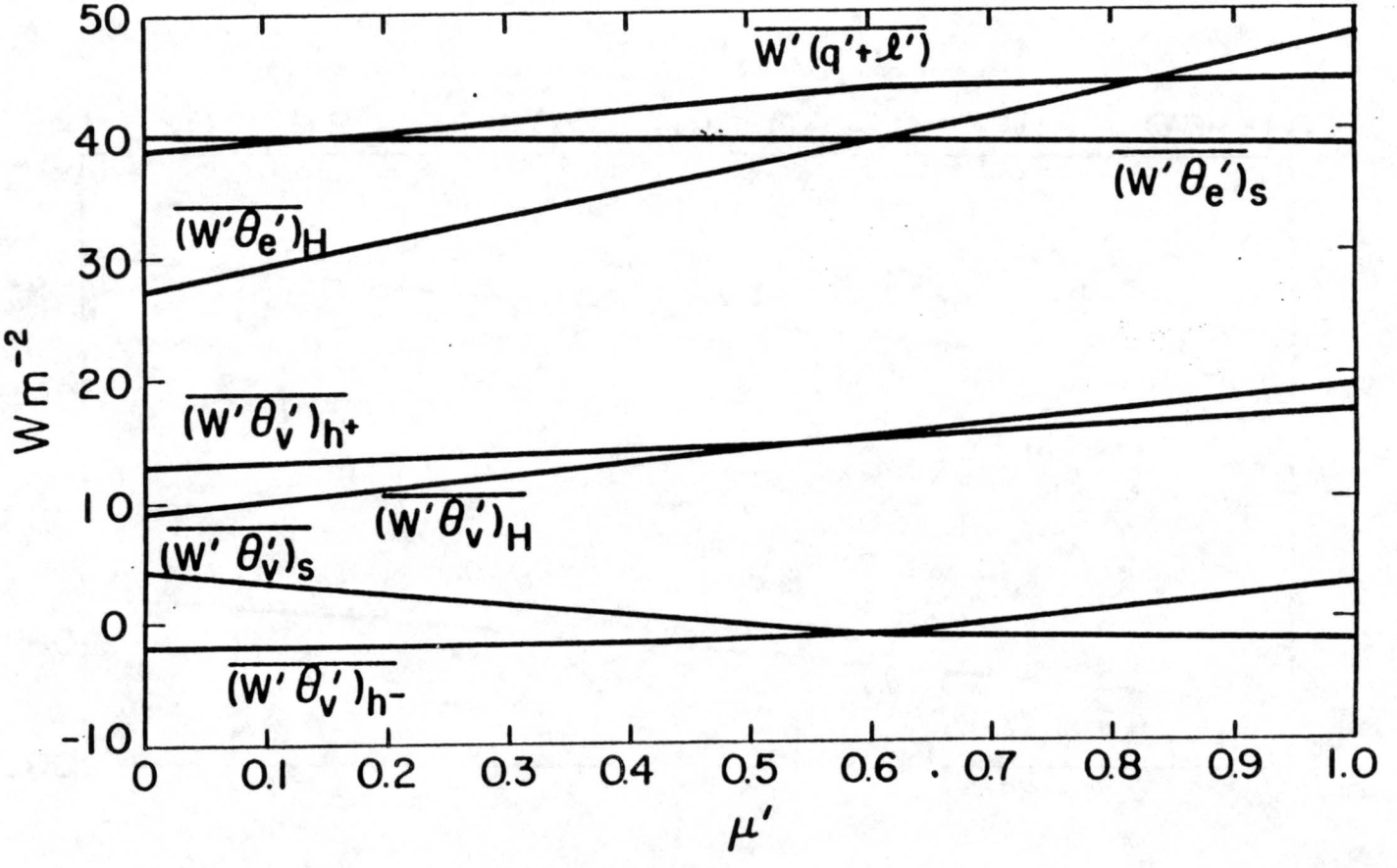

Figure 4.3: Steady-state values of the convective fluxes as a function of the shortwave partition, μ', for closure method one.

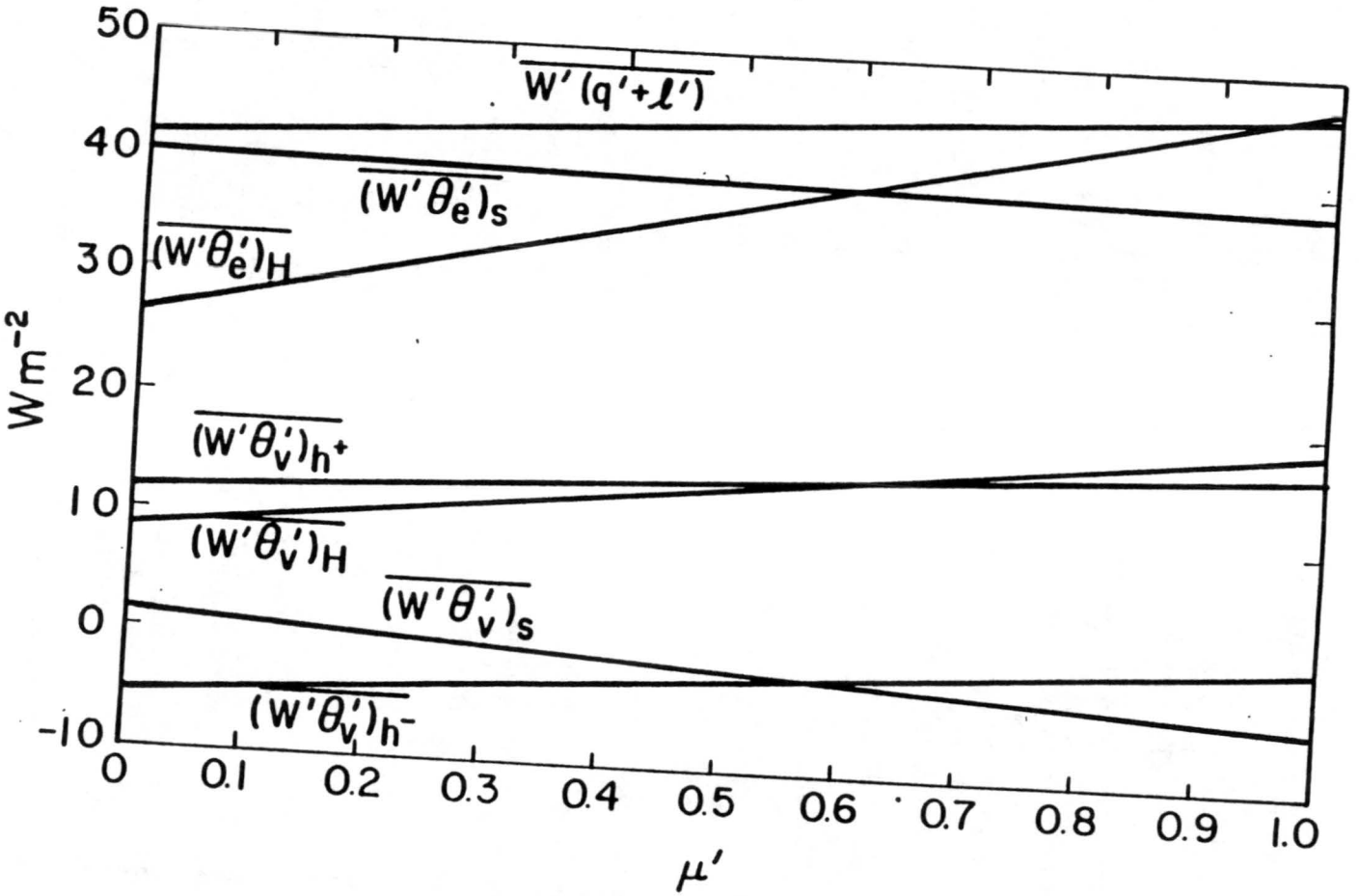

Figure 4.4: Steady-state values of the convective fluxes as a function of the shortwave partition, μ', for closure method two.

boundary layer deepens. In addition, the mixed layer warms causing a rise in the cloud base height. Both Figs. 4.1 and 4.2 clearly show this trend. The main difference between closure methods occurs when the closure equations change to adjust for changes in the $\overline{w'\theta_v'}$ profile. By examining the convective flux curves in Fig. 4.3 it is seen that $(\overline{w'\theta_v'})_{\min}$ changes from just below cloud base to the surface at approximately $\mu' = 0.6$. This change is accompanied by a kink in several of the fluxes. It is also at this point in Fig. 4.1 that a kink appears in both the cloud top and cloud base curves. This kink is attributed to the change in closure equations due to the change in the location of $(\overline{w'\theta_v'})_{\min}$. Closure method two provides much smoother transitions between closure equations. In Fig. 4.4 it is seen that the shape of the $\overline{w'\theta_v'}$ profile changes from that of Fig. 3.2a to that of Fig. 3.2b at approximately $\mu' = 0.3$. There is also a change in profile shape from that of Fig. 3.2b to that of Fig. 3.2c at approximately $\mu' = 1.0$. The difference, however, is that no kinks appear in either the cloud height or convective flux curves at the corresponding points. Because of this smoother transition between closure equations, closure method two is believed to provide a more physically realistic solution to the model.

It should be mentioned that although both models produce physically reasonable trends, the solutions for cloud top and base height appear to be somewhat too low. However, this can be remedied by decreasing the large scale horizontal divergence. As Schubert (1976) noted, halving the divergence approximately doubles the depth of the boundary layer. This result has also been found using this model, as will be shown in the following section. The reason a divergence value of 5.0×10^{-6} s^{-1} has been used is that this value is typical of July Southern California coastal values as taken from the climatological analysis of Neiburger *et al.* (1961).

To further examine the effects of using closure method one versus closure method two, cloud top and cloud base height have been plotted as a function of sea-surface temperature and large-scale divergence for both closure methods. All other variables were held fixed at the following values: wind speed, 7 ms^{-1}; longwave partition, 0.2; shortwave partition, 0.2; entrainment parameter, 0.2; and location, San Diego, CA (Figs 4.5,4.6). Figures 4.5a

and 4.6a show similar trends in that the cloud top height increases as you increase the sea-surface temperature and decrease the divergence. Both Figs. 4.5a and 4.6a agree with Schubert's (1976) finding that the boundary layer depth doubles as you halve the divergence. Closure method two, however, tends to predict higher cloud top and base values than does closure method one and therefore better represents the real atmosphere. Figures 4.5b and 4.6b show similar trends for cloud base height, although cloud base height varies much less as the divergence is decreased. Again, however, closure method two produces higher height values than does closure method one.

4.2 TIME DEPENDENT MODEL EXPERIMENTS AND RESULTS

The first goal in producing time dependent results was to determine which closure method produced the best results. This was done by inputting identical data into both STRATUS Version 2.0 and STRATUS Version 2.1. The following input was used: sea-surface temperature, 16°C; divergence, $5\times10^{-6}s^{-1}$; wind speed, 7 ms^{-1}; longwave radiation partition, 0.2; shortwave radiation partition, 0.4; entrainment parameter, 0.2; and location, San Diego, CA. The results of this experiment were similar to those obtained by the steady-state case. Both closure methods produced the same trends with closure method two predicting higher values of both cloud top and cloud base (Figs. 4.7 and 4.8). The most notable difference was in the $\overline{w'(q'+\ell')}_H$ curve for closure method one (Fig. 4.9). It can be seen from Fig. 4.9 that closure method one produced a kink in the $\overline{w'(q'+\ell')}_H$ curve at approximately 1030 hrs LST. This kink is again associated with the change in closure equations as $(\overline{w'\theta'_v})_{\min}$ goes from just below cloud base to the surface. In Fig. 4.10, the closure equation changes as the $\overline{w'\theta'_v}$ profile changes shape from that of Fig. 3.2a to that of Fig. 3.2b at approximately 0800 hrs LST and again from that of Fig. 3.2b to that of Fig. 3.2c at 1050 hrs LST. However, the fluxes showed no kinks at the corresponding times. Similar results to these were obtained for a variety of input data. For this reason, closure method two was used in the following experiments.

It should be mentioned that some of the results in Fig. 4.9 are physically unrealistic since the $\overline{w'(q'+\ell')}_H$ curve becomes negative. This seems to imply that for a short period

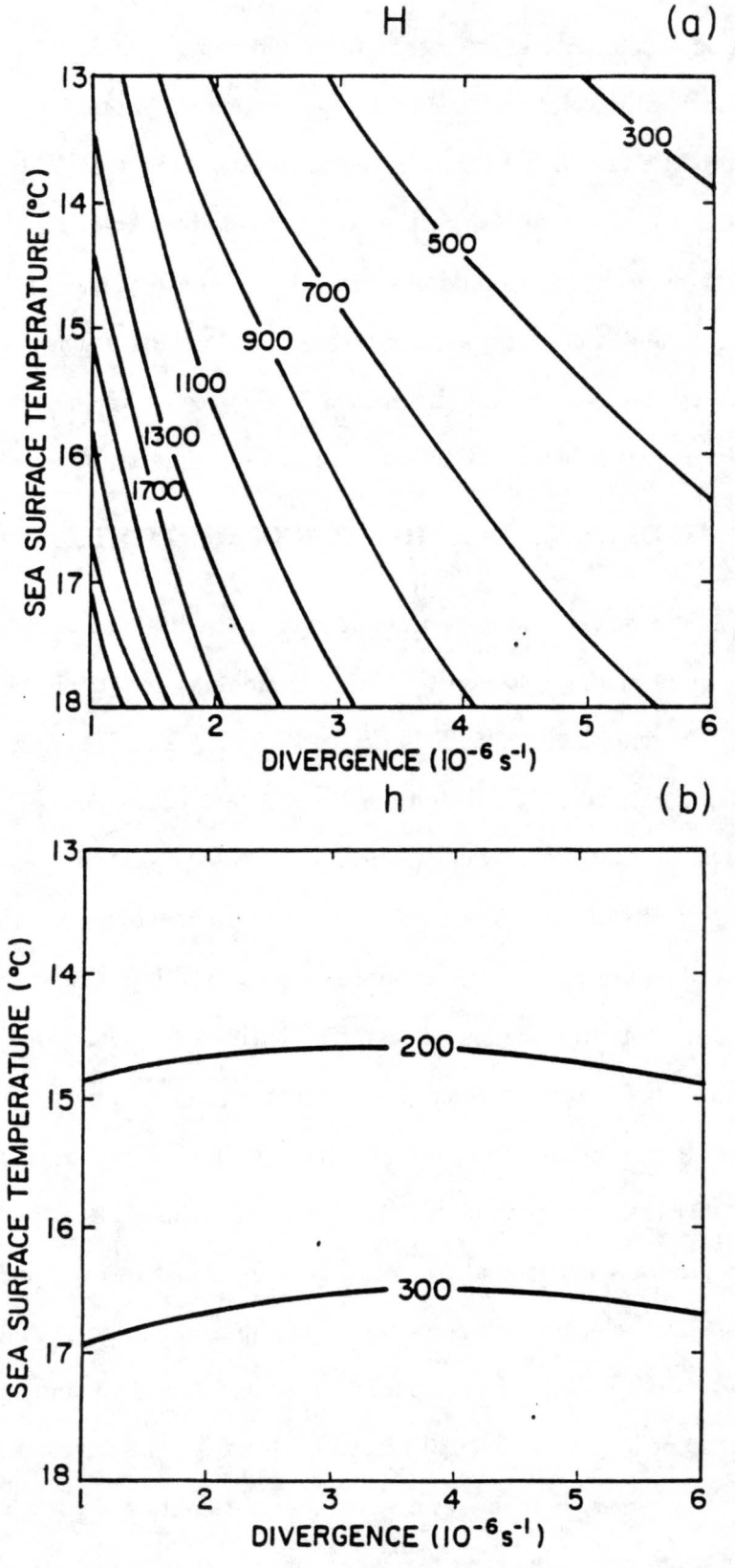

Figure 4.5: Isopleths of (a) cloud top height and (b) cloud base height in meters as a function of sea- surface temperature and large-scale divergence for closure method one.

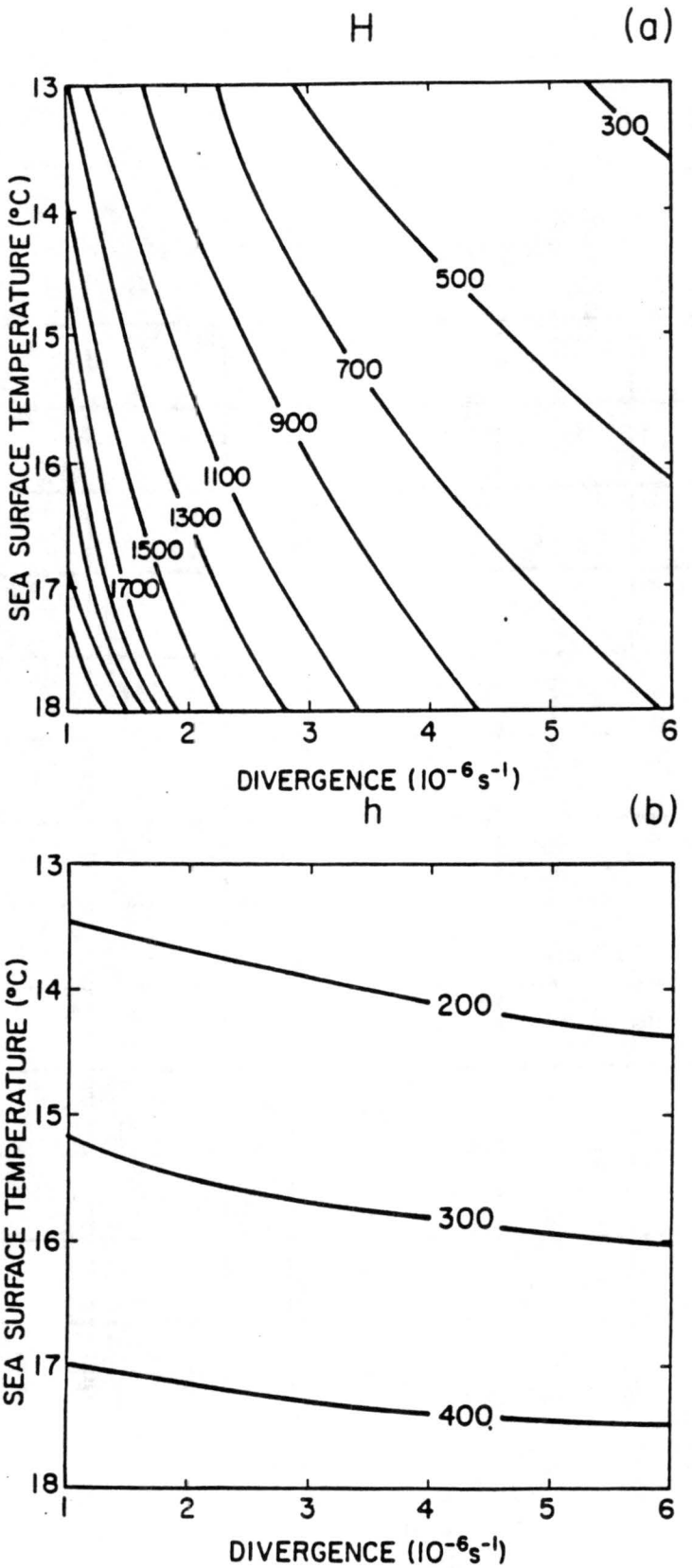

Figure 4.6: Isopleths of (a) cloud top height and (b) cloud base height in meters as a function of sea-surface temperature and large-scale divergence for closure method two.

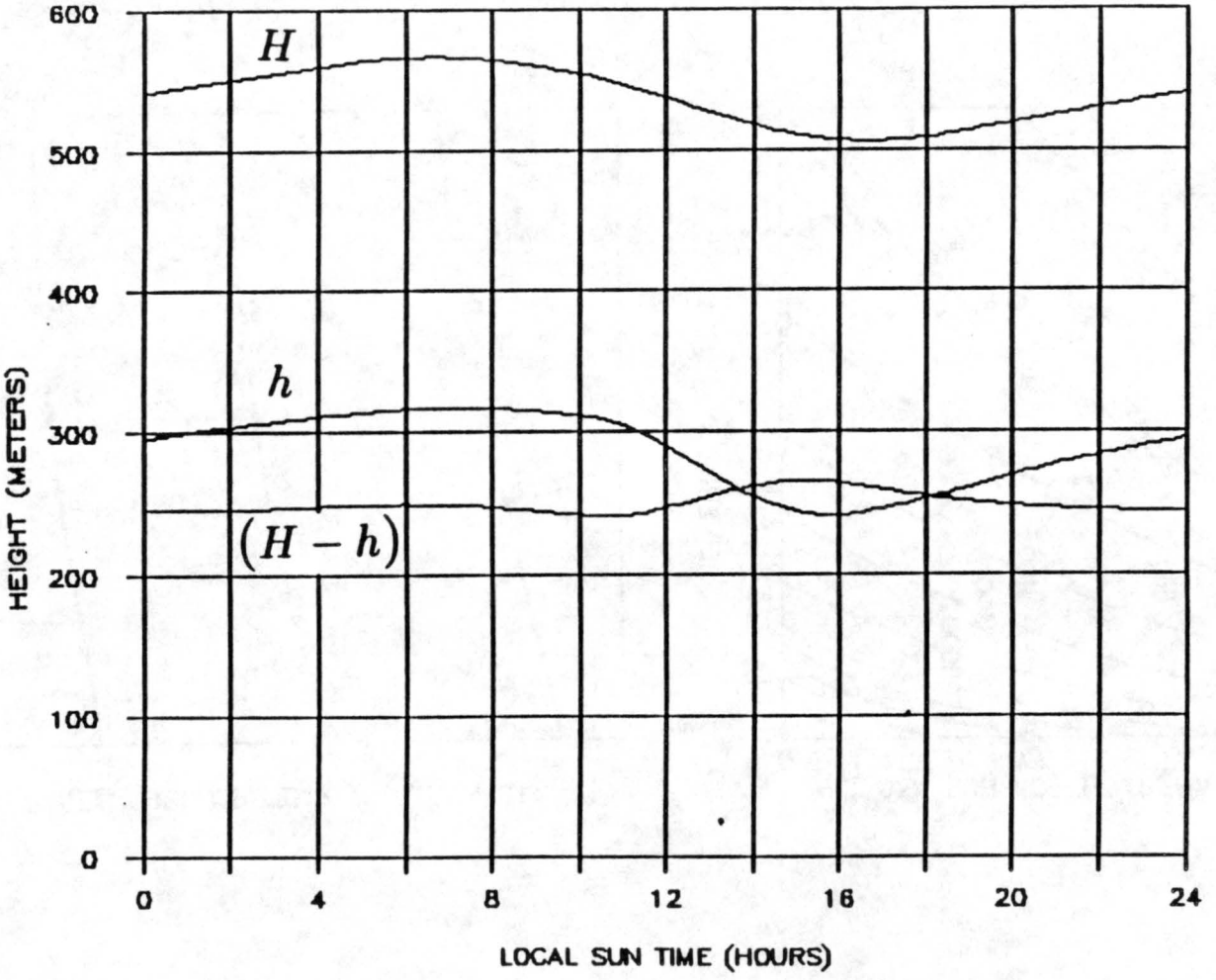

Figure 4.7: Cloud top, base and thickness curves as function of time for closure method one.

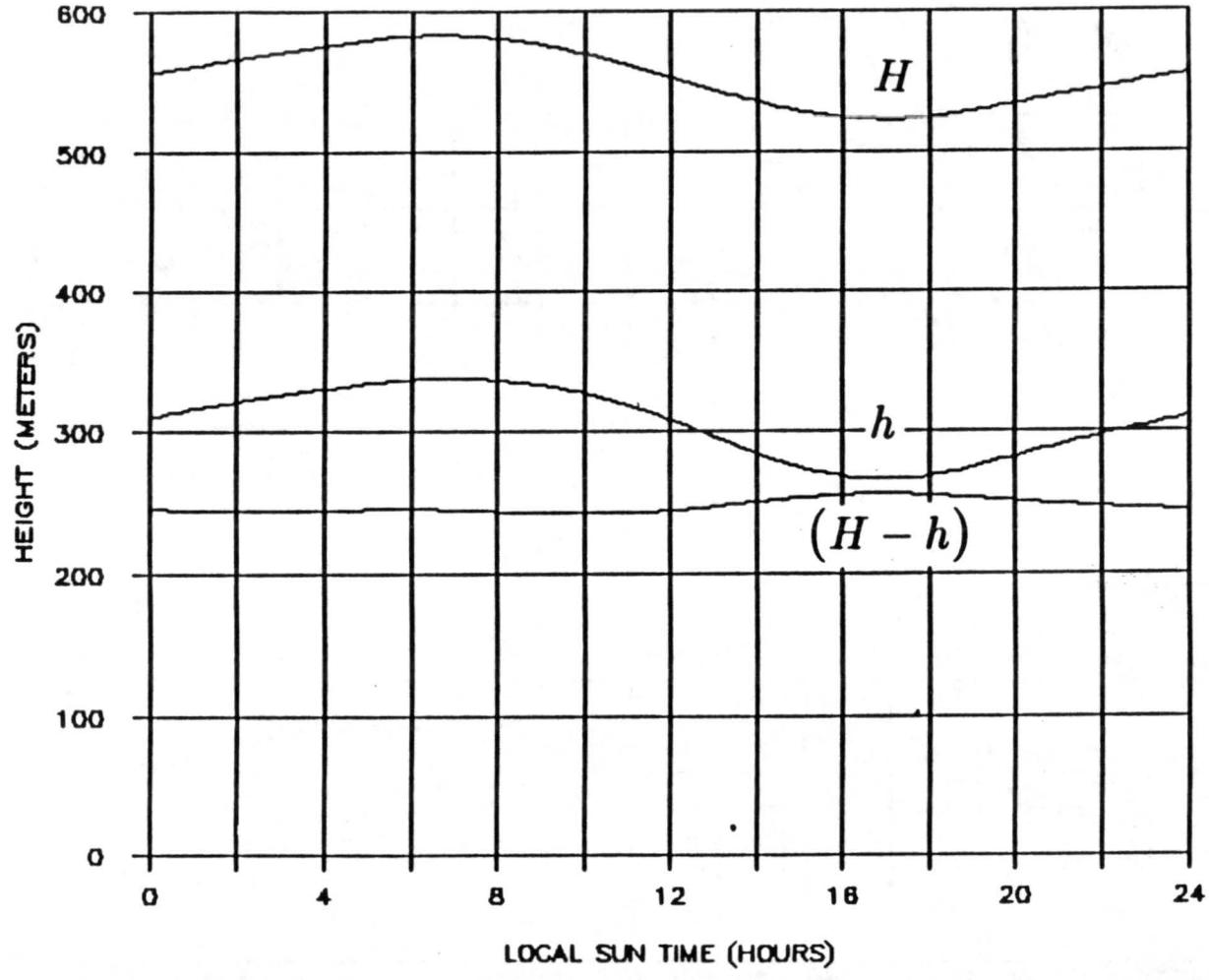

Figure 4.8: Cloud top, base and thickness curves as function of time for closure method two.

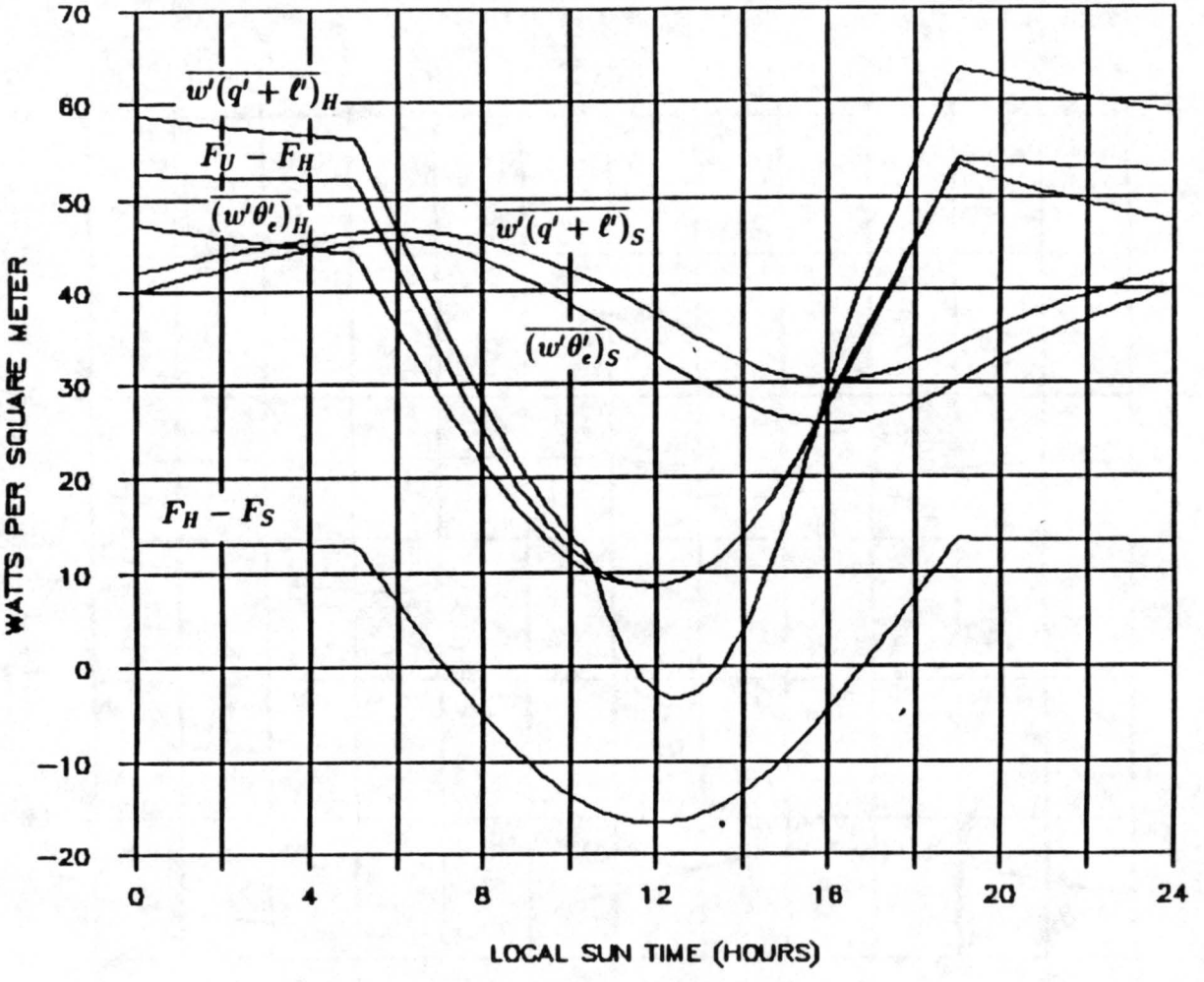

Figure 4.9: Radiative and convective fluxes as function of time for closure method one.

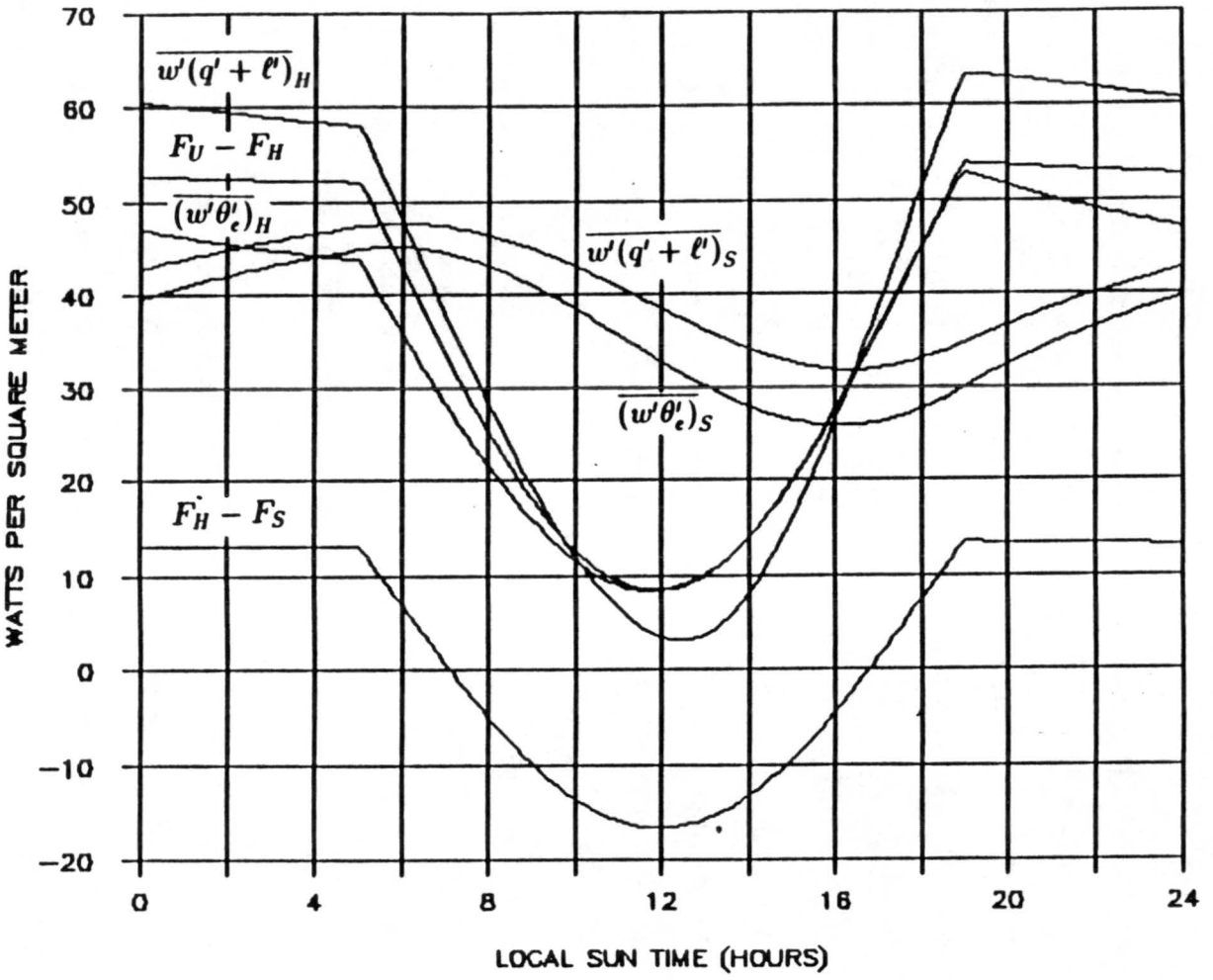

Figure 4.10: Radiative and convective fluxes as function of time for closure method two.

moisture is being supplied from above the inversion which is clearly impossible since we assume this air to be much drier than the mixed layer air. The problem is not that the air above the inversion is more moist that of the mixed layer, but rather it is due to a negative entrainment rate. Because the shortwave partition is relatively small, the majority of the shortwave heating occurs at cloud top. Thus, from (3.44), $F_U - F_H$ becomes small and possibly negative. From (3.50) it is seen that a small or negative value of $F_U - F_H$ will cause $\partial H/\partial t$ to become negative. If $\partial H/\partial t$ is negative and of great enough magnitude, the entrainment rate ($\partial H/\partial t + DH$) can actually become negative (which is physically unreasonable). Thus, from (3.8) it is seen that if the entrainment rate is negative and the air above the inversion is drier than that of the mixed layer (which is the case here), $\overline{w'(q' + \ell')}_H$ will become negative. If we decrease the shortwave partition slightly, closure method two will also display this same feature. On the other hand, if we increase the shortwave partition we can completely remove this feature.

The next set of experiments looks at the theoretical effects of the diurnal cycle on the growth and dissipation of the horizontally homogeneous marine stratocumulus cloud layer as calculated by STRATUS Version 2.1. The modeling results are compared with observational results obtained by Betts (1989) and Davies and Blaskovic (1988).

Betts (1989) completed an observational study of this phenomena using sounding and ceilometer data collected on San Nicolas Island off the southern California Coast for the First ISCCP (International Satellite Cloud Climatology Project) Regional Experiment (acronym FIRE) (Albrecht *et al.*, 1988). The data represented the two day period July 10–12, 1987, during which light winds ($V \leq 5.0$ ms^{-1}) prevailed. Figure 4.11 is a graph of Betts' (1989) analysis for the two day period which clearly shows a thinning of the cloud layer during the afternoon hours; this is due primarily to the rapid rise of cloud base depth and relatively invariant cloud top height. Similar results were also obtained by Davies and Blaskovic (1988) in which the diurnal variation in cloud thickness was observed over the whole FIRE experiment (July 1–19, 1987) using both columnar liquid water content measurements and ceilometer data combined with sounding data (Figs. 4.12a,b). These

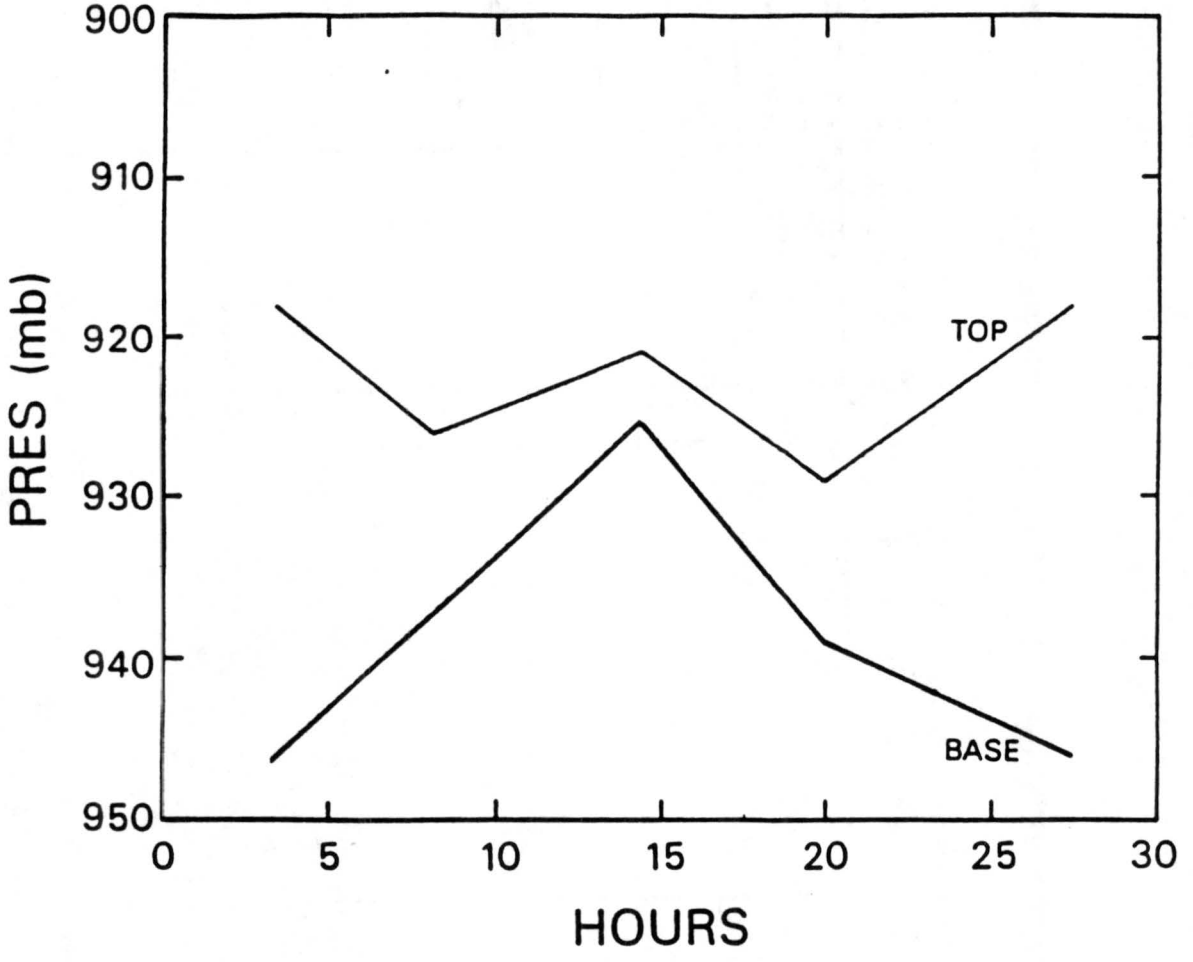

Figure 4.11: Observational results of cloud top and base height as a function time (PST). After Betts (1989).

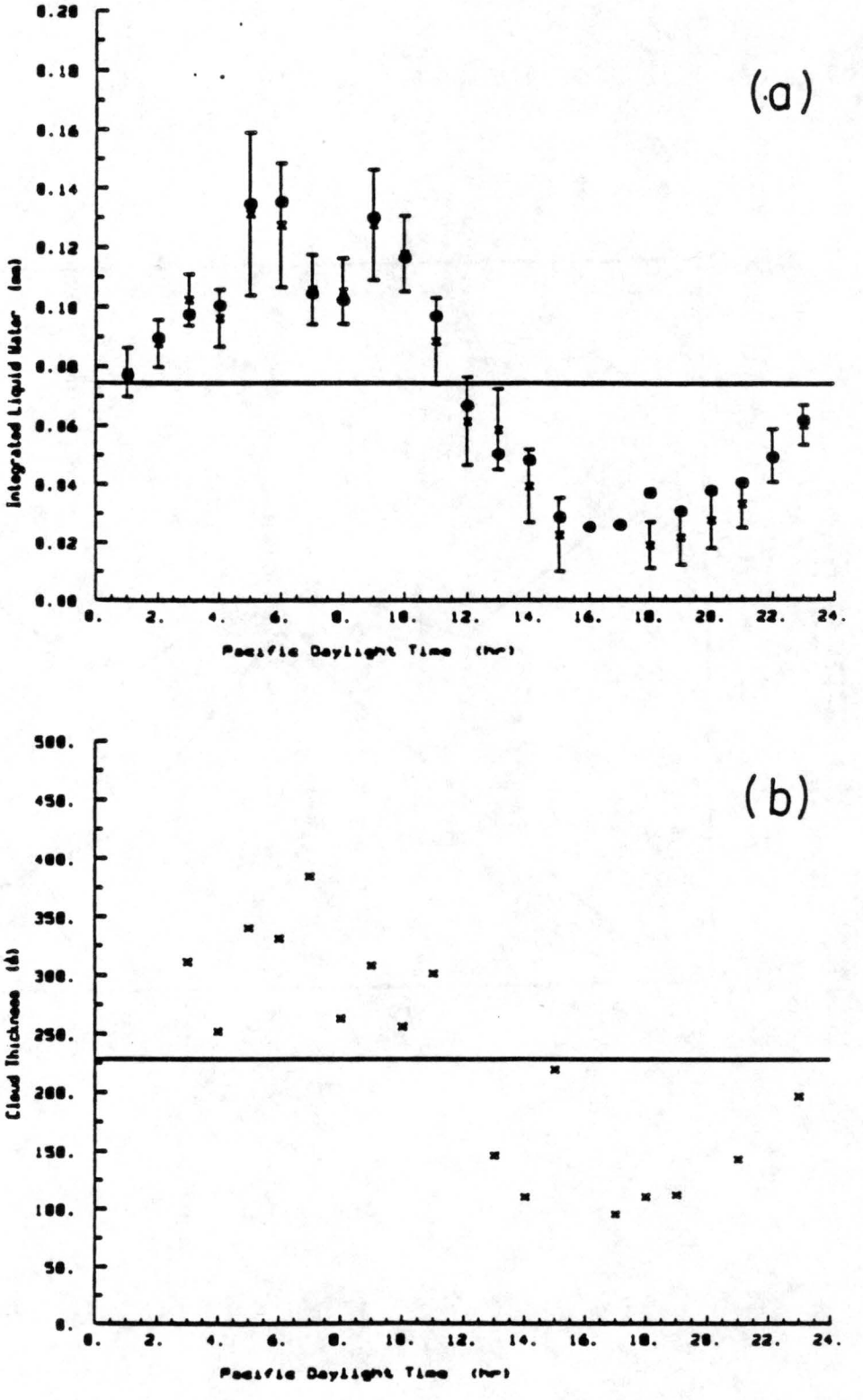

Figure 4.12: Observational values of (a) column liquid water as determined by the NOAA/WPL radiometer and (b) cloud thickness as determined by ceilometer and radiosonde data as a function of time (PST). From Davies and Blaskovic (1988).

figures indicate that the cloud thickness reaches a maximum value of 400m during the morning hours and thins to approximately 28m during the late afternoon.

This afternoon "burn off" of the cloud is not detectable in the modeling results. It can be seen from Fig. 4.7 that although cloud base rises during the maximum solar heating period, the cloud thickness remains relatively invariant with time due to the diurnal change in cloud top height. Thus, it would seem that the afternoon burn off of the stratocumulus clouds is not valid under these conditions. However, by allowing the majority of the shortwave radiation to penetrate into the mixed layer, the variance of the longwave cooling with time is decreased and therefore the variance of cloud top height with time is decreased as is shown by equation (3.50). At the same time, the variance with time of the mixed layer heating is increased and therefore the variance of cloud base height with time is increased. In short, we can maintain a constant cloud top height and allow the cloud base to rise simply by increasing μ'. The end result is an afternoon thinning of the cloud layer. To demonstrate this, Fig. 4.7 has been recalculated using a μ' of 0.8 instead of 0.4. The result is shown in Fig. 4.13.

Figure 4.13 clearly shows an afternoon thinning of the cloud layer. The cloud thickness reaches its minimum value at approximately 1400 hrs LST which roughly corresponds to Betts (1989) and Davies and Blaskovic (1988) observational values. Similar patterns of diurnal thinning (although of differing magnitude) are reproduced by the mixed layer model of Hanson and Gruber (1982) in which the shortwave absorption coefficient is allowed to change based on the cloud liquid water content.

Although our model accurately predicts the thinning trend, the magnitude of the change in thickness is largely underpredicted. Even if μ' is increased to 1.0 the change in thickness still goes largely underpredicted. In an attempt to solve this problem, the shortwave absorption coefficient was increased from its value of 7% to a value of 12.4% corresponding to a mean of the values calculated by Duda (1989) using data from July 8 and 10, 1987, for the FIRE project. The specific values Duda (1989) calculated were 14.4±3.5 for July 8 and 10.4±4.4 for July 10. The reason for increasing the shortwave

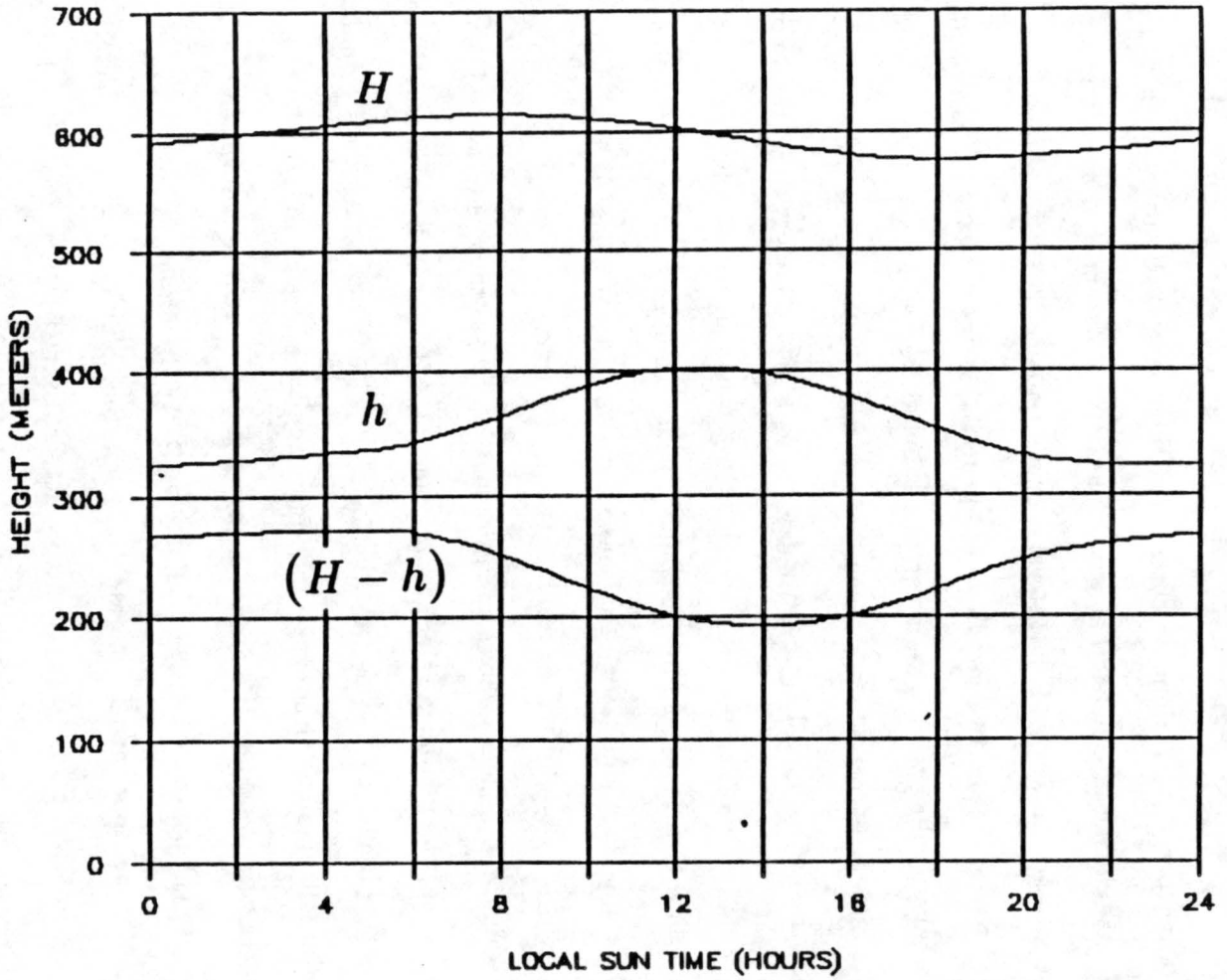

Figure 4.13: Cloud top, base and thickness curves as a function of time with an increased μ' of 0.8.

radiation absorption coefficient was to increase the magnitude of the variability in the cloud base height. The result of this, however, was model output with no physical meaning. In all cases but one where a shortwave absorption coefficient of 12.4% was used, $\overline{w'(q' + \ell')}_H$ became negative during the maximum heating period. The reason for this stems from the enormous magnitude of the shortwave absorption which again causes $F_U - F_H$ to become negative during the maximum solar heating period for all cases except when $\mu' = 1.0$. The end result is a negative entrainment rate which forces $\overline{w'(q' + \ell')}_H$ to be negative. In a further attempt to increase the thinning of cloud base, a shortwave absorption value of 10% was used. Although the problem of a negative $\overline{w'(q' + \ell')}_H$ was eliminated for a wider range of input data, the results differed little from those obtained for a shortwave absorption value of 7%. This seems to be a limitation of mixed layer models in general. In a higher order modeling study by Bougeault (1985) which discretizes the boundary layer into several levels, it was found that during the period of maximum solar heating the mixed layer actually became separated by a slightly stable region. Observational studies by Betts (1989) have also shown the diurnal separation of the mixed layer. This formation of a stable layer acts to turn off the vapor flux which decreases the liquid water content of the cloud layer and thus aids the diurnal thinning of the cloud. A mixed layer model, however, is unable to handle such a separation of layers and therefore the thinning of the cloud layer is limited only to radiative effects. Because of the problems encountered when the shortwave absorption coefficient is increased, the diurnal cycle in our remaining experiments is represented by using a shortwave absorption coefficient of 7% and a μ' of 0.8

One final feature of the diurnal cycle that has been simulated is its influence on thin clouds versus thick clouds. The case of a relatively thin cloud is first considered. To produce a thin cloud the wind speed of the previous case is decreased to 5 ms^{-1}. This decreases the moisture flux upward from the sea-surface. The result, shown in Fig. 4.14, is a cloud layer which varies from 180 m in thickness during the morning to 70 m at 1500 hrs LST. This equates to a diurnal thinning of 110 m. These results are quite different for

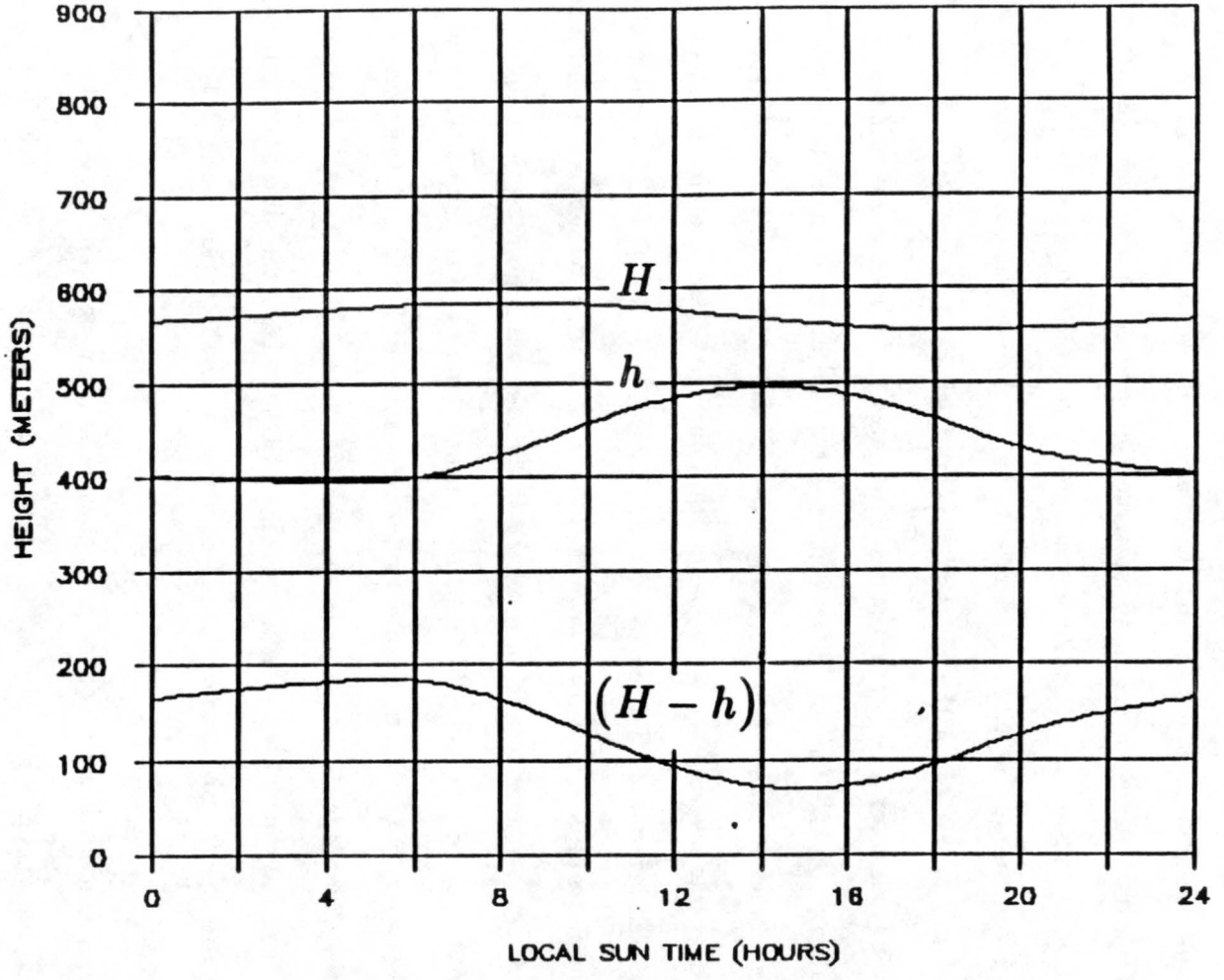

Figure 4.14: Cloud top, base and thickness curves as a function of time for the thin cloud case.

the thick cloud case. To generate a thick cloud, the sea-surface temperature is increased to 17 °C, the large-scale divergence is decreased to 4.5×10^{-6} s^{-1} and the wind speed is increased to 10 ms^{-1}. This has the effect of raising the boundary layer depth by warming the mixed layer and decreasing the entrainment of dry air from above the inversion, and lowering the cloud base height by increasing the flux of moisture from the surface. These results are shown in Fig. 4.15. As one would expect, the effect of the diurnal cycle is much less for the thick cloud. The thick cloud varies in thickness by only less than 50 m. The reason the thick cloud shows a smaller variation in thickness is that the flux convergence of heat in the mixed layer is large due to the increased surface temperature so that the mixed layer radiative flux divergence has less of an influence on the change in θ_e. The result is a cloud base which varies little in time, which can be seen from (3.40) and (3.48).

It should be mentioned that in several of the above results $\Delta\theta_e$ became negative. This is a clear violation of Lilly's (1968) cloud top stability condition. However, Randall (1980) gives a more accurate stability condition that includes virtual temperature effects. Under this stability condition, the cloud layer remains stable until $\Delta\theta_e$ becomes appreciably negative. Typical values are on the order of -2 degrees. In none of the above cases did $\Delta\theta_e$ fall below this value. They were therefore accepted as real solutions.

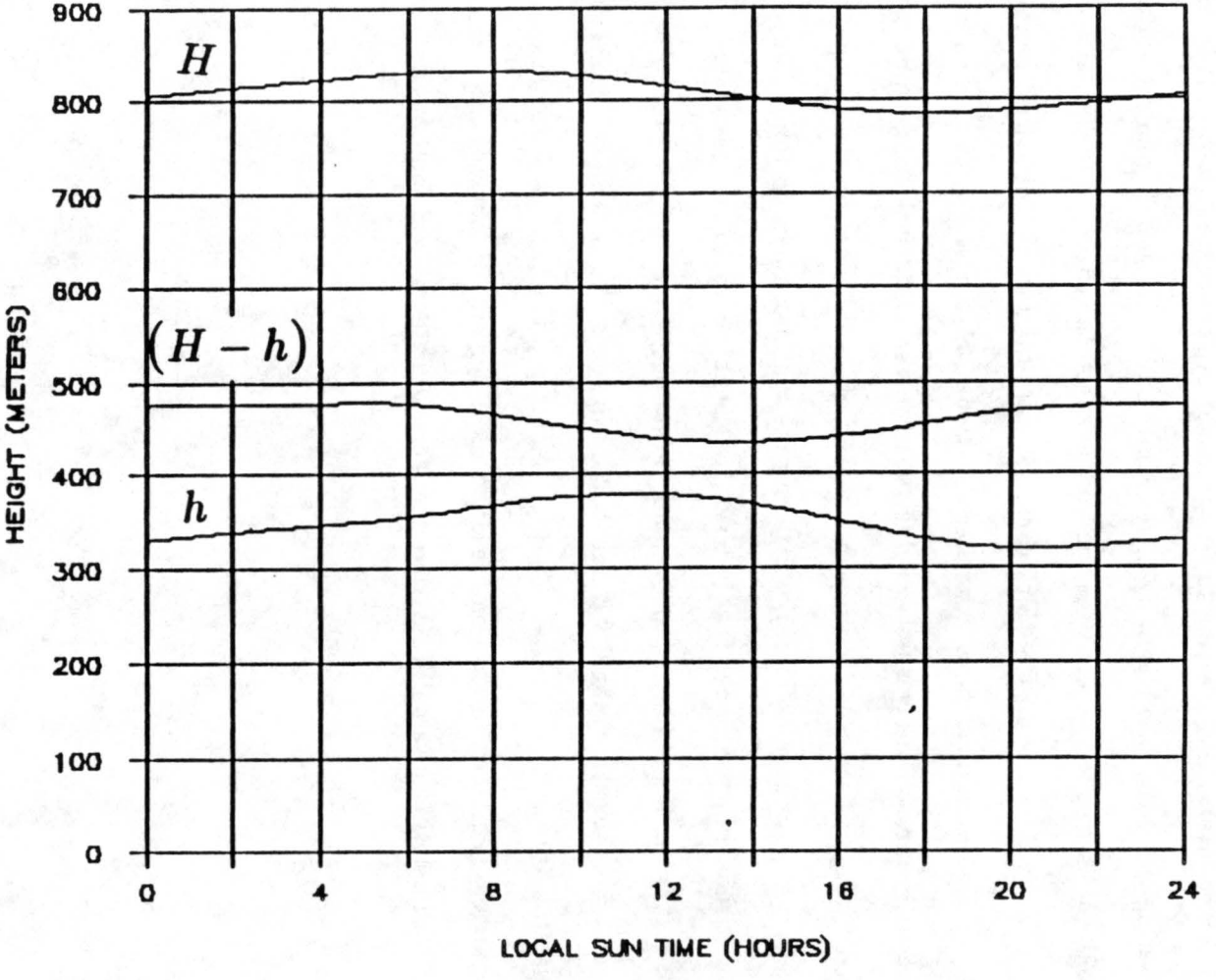

Figure 4.15: Cloud top, base and thickness curves as a function of time for the thick cloud case.

Chapter 5

SUMMARY AND CONCLUSIONS

In this report Lilly's (1968) mixed layer model has been generalized to include the effects of penetrating both longwave and shortwave radiation into the mixed layer in an attempt to simulate the diurnal cycle. In addition to this, two closure assumptions have been used: one which is a weighted mean of Lilly's maximum and minimum entrainment hypotheses and one which considers the ratio of the integral buoyant energy dissipation over the integral buoyant energy production to be a constant. The conservative thermodynamic variable, equivalent potential energy, was used instead of moist static energy in order to help broaden the audience of the report.

Modeling studies for both the steady-state and time-dependent solutions for both closure assumptions were completed. The steady-state results indicated that both closure assumptions provided similar results for the same input data. Closure method two provided a much smoother transition between closure equations which vary with the virtual potential temperature flux profile. Because of its smoother transition between closure equations, it is believed that closure method two provides more realistic solutions to the real environment. It was also noted that closure method two produced cloud depths that were slightly closer to that of the real atmosphere.

The time-dependent results were used to both intercompare both closure assumptions as well as to investigate the diurnal thinning of the marine stratocumulus clouds. Results indicated again that for the same entrainment parameter, both closures produce similar results. As with the steady state case, however, closure method one generates kinks in the output when the model switches from one virtual potential temperature flux profile to another.

Results from experiments of the simulation of the diurnal cycle were successful. By allowing the majority of the shortwave radiation to penetrate into the mixed layer, a diurnal thinning trend similar to the observational results of Betts (1988) and Davies and Blaskovic (1988) could be produced. Although the modeled thinning occurred at the observed times, it was much less in magnitude. In an attempt to correct this, a stronger shortwave absorption coefficient was used. This, however, resulted in physically unreasonable results.

The effects of the diurnal cycle were also modeled for relatively thick clouds versus relatively thin clouds. The model results indicated that thin clouds were much more susceptible to diurnal thinning than were the thick clouds. In this study the thin clouds showed a decrease in thickness which was twice as great as that of the thick clouds for the same radiation partition.

Although the results show the relative success of our mixed layer models, they also show their limitations. The greatest success comes from the models' ability to accurately simulate the trends of the diurnal cycle, whereas its primary limitation lies with its inability to represent a separation of the mixed layer. This separation is caused by the intense warming and consequent stabilizing of the mixed layer which occurs during the intense afternoon solar heating. When the separation takes place, the flux of moisture from the ocean surface to the cloud layer is effectively shut off. The end result is a thinning of the cloud layer which is much greater than if only radiative effects were considered. It may be that accurate simulations of the magnitude of the diurnal thinning are limited to higher order models such as that of Bougeault (1985). These higher order models contain multiple levels and thus can simulate the diurnal separation of the mixed layer. Mixed layer models will, however, remain an important academic and research tool because of their simplicity and computational efficiency. Although their use may be somewhat limited, they will still be useful in quickly assessing the importance of the predictive variables as well as their influence upon each other. They will also remain useful in determining the accuracy of

various new methods of paramaterizing the complex physical processes which govern the marine boundary layer.

REFERENCES

Albrecht, B.A. and R.S. Penc, 1985: An observational study of cloud-topped mixed layers. *J. Atmos. Sci.*, **42**, 800–822.

——, D.A. Randall and S. Nicholls, 1988: Observations of marine stratocumulus during FIRE. *Bull. Amer. Meteor. Soc.*, **69**, 618–626.

Betts, A.K., 1989: Diurnal variation of California coastal stratocumulus from two days of boundary layer soundings. *Tellus*, **41A**, in press.

Bougealt, P., 1985: The diurnal cycle of the marine stratocumulus layer: A higher order model study. *J. Atmos. Sci.*, **42**, 2826–2843.

Cox, S.K., 1973: Infrared heating calculations with a water vapor pressure broadened continum. *Quart. J. R. Meteor. Soc.*, **99**, 669–679.

Davies, R. and M. Blaskovic, 1988: Diurnal variation of marine stratocumulus over San Nicholas Island during the FIRE IFO. FIRE Science Team Workshop report, Vail, CO. July 11–15, 1988, 209–213.

Duda, D.P., 1989: Microphysical and radiative properties of marine stratocumulus from tethered balloon measurements. M.S. Thesis, Colorado State University, Ft. Collins, CO 80523. 120pp.

Hanson, H.P. and P.L. Gruber, 1982: Effect of marine stratocumulus clouds on the ocean-surface heat budget. *J. Atmos. Sci.*, **39**, 897–908.

Kraus, H. and E. Schaller, 1978a: Steady-state characteristics of inversions capping a well mixed boundary layer. *Boundary-Layer Meteor.*, **14**, 83–104.

—— and ——, 1978b: A note on the closure in Lilly-type inversion models. *Tellus*, **30**, 284–288.

Lilly, D. K., 1968: Models of cloud-topped mixed layers under a strong inversion. *Quart. J. R. Meteor. Soc.*, **94**, 292–309.

Lowe, P.R., 1977: An approximating poynomial for the computation of saturation vapor pressure. *J. Appl. Meteor.*, **16**, 100–103.

Manabe, S. and R.T. Wetherald, 1967: Thermal equilibrium of the atmosphere with a given distribution of relative humidity. *J. Atmos. Sci.*, **24**, 241–259.

Neiburger, M., 1949: Reflection, absorption and transmission of isolation by stratus cloud. *J. Met.*, **6**, 98–104.

——, D.S. Johnson and C. Chein, 1961: Studies of the structure of the atmosphere over the eastern pacific ocean in summer. *Univ. Calif. Pub. Meteor.*, **1**, 1–94.

Randall, D.R., 1980: Conditional Instability of the First Kind Upside-Down. *J. Atmos. Sci.*, **37**, 125–130.

——, J.A. Coakly, Jr., C.W. Fairall, R.A. Kropfli and D.H. Lensschow, 1984: Outlook for research on subtropical marine stratiform clouds. *Bull. Amer. Meteor. Soc.*, **65**, 1290–1301.

——, J.A. Abeles and T.G. Corsetti, 1985a: Seasonal simulations of the planetary boundary layer and boundary layer stratocumulus clouds with a general circulation model. *J. Atmos, Sci.*, **42**, 641–675.

——, 1985b: Key problems of paramaterization for simple cloud-topped boundary layer models. A paper presented at the Workshop on the Modelling of the Cloud-Topped Boundary Layer of the World Climate Research Program, Fort Collins, CO, April, 1985.

Schubert, W. H., 1976: Experiments with Lilly's cloud-topped mixed layer model. *J. Atmos. Sci.*, **33**, 436–445.

——, J.S. Wakefield, E.J. Steiner and S.K. Cox, 1979: Marine stratocumulus convection. Part I: Governing equations and horizontally homogeneous solutions. *J. Atmos. Sci.*, **36**, 1286–1307.

Slingo, A., S. Nicholls and J. Schmetz, 1982: Aircraft Observations of marine stratocumulus during JASIN. *Quart. J. R. Meteor. Soc.*, **108**, 833–856.

U. S. Dept. of Commerce, Enviromental Science Services Administration, Enviromental Data Service, 1976–1980: *Climatological Data, National Summary.* Govt. Printing Office, Washington, D.C.

APPENDIX

In this appendix the linear condensation equation (2.1) and its coefficients are derived. We begin by first defining the equation for the saturation vapor mixing ratio (q_{sat}) which is a function of both temperature and pressure as

$$q_{\mathrm{sat}}(T,p) = \frac{0.622 e_s(T)}{p - e_s(T)}, \tag{A.1}$$

where T is temperature, p is pressure, and $e_s(T)$ is the saturation vapor pressure for a given temperature. Since q_{sat} depends only on T and p, it can be expressed linearly in differential form as

$$dq_{sat} = \left(\frac{\partial q_{sat}}{\partial T}\right)_p dT + \left(\frac{\partial q_{sat}}{\partial p}\right)_T dp. \tag{A.2}$$

Equation (A.2) is a linear differential equation for q_{sat} in terms of temperature and pressure. However, since (2.1) is in terms of potential temperature θ and physical height z, (A.2) needs to also be expressed in terms of θ and z. The conversions of the differential of temperature to the differential of potential temperature and the differential of pressure to the differential of height can easily be accomplished through use of Poisson's equation and the hydrostatic approximation.

By taking the logarithmic derivative of Poisson's equation it can be shown that

$$dT = \frac{T}{\theta} d\theta + \frac{RT}{c_p p} dp, \tag{A.3}$$

where R is the gas constant for dry air and c_p is the specific heat at constant pressure for dry air, and from the hydrostatic equation, we can see directly that

$$dp = -\rho g dz, \tag{A.4}$$

where ρ is the air density and g is gravity.

By substituting (A.3) and (A.4) into (A.2) while making use of the ideal gas law, (A.2) can be written as

$$dq_{sat} = \frac{T}{\theta}\left(\frac{\partial q_{sat}}{\partial T}\right)_p d\theta - g\left\{\frac{1}{c_p}\left(\frac{\partial q_{sat}}{\partial T}\right)_p + \frac{p}{RT}\left(\frac{\partial q_{sat}}{\partial p}\right)_T\right\} dz. \qquad (A.5)$$

The partial derivatives in (A.5) are determined through use of (A.1). The term $(\partial q_{sat}/\partial T)_p$ is determined by differentiating (A.1) with respect to temperature while holding pressure constant. The result of doing this is

$$\left(\frac{\partial q_{sat}}{\partial T}\right)_p = 0.622\frac{\partial e_s}{\partial T}\frac{p}{(p-e_s)^2} = q_{sat}\left(\frac{p}{p-e_s}\right)\frac{\partial \ln e_s}{\partial T}. \qquad (A.6)$$

However, from the Clausius-Clapeyron equation, we see that

$$\frac{\partial \ln e_s}{\partial T} = \frac{L}{R_v T^2}, \qquad (A.7)$$

where L is the latent heat of evaporation and R_v is the gas constant for water vapor. Substituting (A.7) into (A.6) gives

$$\left(\frac{\partial q_{sat}}{\partial T}\right)_p = \frac{L q_{sat}}{R_v T^2}\left(\frac{p}{p-e_s}\right) \qquad (A.8)$$

To determine the term $(\partial q_{sat}/\partial p)_T$, (A.1) is differentiated with respect to pressure while holding temperature constant. The result is

$$\left(\frac{\partial q_{sat}}{\partial p}\right)_T = -\frac{0.622 e_s}{(p-e_s)^2} = -\frac{q_{sat}}{p-e_s}. \qquad (A.9)$$

Finally, by substituting (A.8) and (A.9) into (A.5) the desired expressions for the coefficients a and b are obtained. These are

$$a = \frac{L q_{sat}}{R_v T\theta}\left(\frac{p}{p-e_s}\right),$$

and

$$b = \frac{gpq_{sat}}{(p-e_s)c_p}\left(\frac{L}{R_v T^2} - \frac{c_p}{RT}\right),$$

where the units for a and b are deg^{-1} and m^{-1} respectively.

The calculations of a and b are straightforward with the exception of determining e_s. To determine e_s for model computations, an algorithm written by Lowe (1977) is used.